wax, and 15% plasticizing materials) were compounded in a tumbler mixer (Neo TecsK03P), and then mixed at room temperature in a rotating drum tumbler mixer for 5 h.

2.1.2. Fabrication of Tetrabones

Injection molds were prepared to fabricate 1 mm sized tetrapods, and the α-TCP powders were molded using an injection molding machine (J34AD, Japan Steel Works, Tokyo, Japan). Molded products were then degreased and calcined. The detailed parameters for the injection molding, degreasing, and calcination processes are given in Table 1.

The degreased and calcined products were soaked in 0.2 M succinic acid for 24 h to form octacalcium phosphate (OCP), rinsed twice with distilled water, dried under reduced pressure, and sterilized by electron beam irradiation at 25 kGy to give the final Tetrabone product.

β-TCP granules (Osferion®, size range 0.5–1.5 mm, porosity 75%; Olympus Biomaterial Corp., Tokyo, Japan) were used as the control material.

2.2. Material properties of Tetrabones

2.2.1. X-ray diffraction analysis

X-ray diffraction analysis (XRD) was performed using an X-ray diffractometer (Mini Flex 2, Rigaku, Japan) equipped with a CuK_α radiation source at 20 mA, scanning from $2\theta = 4$ to 60 °C. All samples were crushed before analysis. The results were compared with the International Center for Diffraction Data (ICDD) database.

2.2.2. Scanning electron microscopy

Scanning electron microscopy (SEM) was performed on pure α-TCP powders and the surface of injectionmolded products before and after succinic acid treatment, using a JCM-5700 scanning electron microscope (JEOL, Tokyo, Japan). Images were obtained at 1.2 keV accelerating voltage and 20 mA current.

2.2.3. Mechanical testing

The rupture strength of single Tetrabones and single β-TCP granules were measured with a rheometer (CR-500DX, Sun scientific Co., Japan). A single particle of each artificial bone was placed on the slab of the rheometer. The rod was loaded at 3 mm min^{-1} until the particle ruptured, and the rupture strength when each specimen broke was measured ($n = 4$).

For elastic modulus evaluation Tetrabones and β-TCP granules were embedded in cylindrical molds 5 mm in diameter and 10 mm long, and each mold was placed on the slab of an Instron universal testing machine (Instron-3365, Instron Corp., Norwood, MA). Arod 5 mm in diameter was loaded into the mold at 0.5 mm min^{-1}, and the elastic modulus measured ($n = 4$).

2.2.4. Analysis of size and connectivity of intergranular pores

Polymer beads used to simulate cells and blood vessels were provided by the Sekisui Plastics Corporation (Osaka, Japan). The beads were composed of cross-linked polymethyl methacrylate and had diameters of 100, 300, 400, and 600 μm.

The end of a 2.5 ml syringe barrel was cut to create a cylindrical tube and sealed with mesh. The plunger was pulled back and the rubber cap removed. The barrel was filled with 0.5 ml of Tetrabones or β-TCP granules, overlaid with 1.5 ml of the beads, and the plunger pushed back into the barrel. The end of the plunger was loaded with a 500 g weight and the syringe was vibrated using a vibrator for 2 min. The beads were collected as they exited the syringe and their weight measured ($n = 3$, Fig. 1). Additionally, mercury porosimetry was performed using a Micromeritics Autopore III 9510 mercury porosimeter (Micromeritics Instrument Corp., Norcross, GA) to compare the values of these methods.

Table 1
Detailed parameters of the Tetrabone fabrication process.

Injection molding	Degreasing	Calcination
Cylinder temperature 170–190 °C	Maximum temperature 500 °C	Maximum temperature 700 °C
Mold temperature 25–40 °C	Rate of temperature rise 87°Ch^{-1}	Rate of temperature rise 87°Ch^{-1}
Injection pressure 30–50 MPa	Holding time 1 h	Holding time 1 h
Injection velocity 0.3–0.5 s		
Screw revolution speed 1000 r.p.m.		

2.2.5. Cell viability

MC3T3-E1 cells were cultured on Tetrabones or β-TCP granules in standard medium (Dulbecco's modified Eagle's medium (DMEM) supplemented with 10 vol.% fetal bovine serum (FBS), 50 U ml^{-1} penicillin, and 50 mg ml^{-1} streptomycin) at 37 °C in a 5% CO_2 atmosphere. When the cells reached confluence the medium was changed to osteogenic medium (standard medium supplemented with 0.1 μM dexamethasone, 50 mM β-glycerophosphate and 50 μg ml^{-1} ascorbic acid). 7 days later the Tetrabones and β-TCP granules were stained with an alkaline phosphatasestaining kit (Takara Bio, Tokyo, Japan). The numbers of cells growing on the surface of the Tetrabones and β-TCP granules werecounted using a stereoscopic microscope.

2.3. In vivo experiments

2.3.1. Canine bone defect model

Seven healthy beagle dogs (10–12 kg body weight, 1–2 years of age) were purchased from Nosan Corporation (Kanagawa, Japan). General anesthesia was maintained with isoflurane, and fentanyl hydrate was continuously administered during and after surgery. The femoral medial condyle was exposed, and a tunnel defect 10 mm in diameter extending to the lateral cortex was created in the bilateral femur using a power surgery drill (IMEX™ Veterinary Inc., Longview, TX). After irrigation of the defect with sterile saline, Tetrabonesor β-TCP granules were implanted into the defect ($n = 5$ each), or, in the control group, nothing was implanted ($n = 4$). After implantation the joint capsule, fascia lata, subcutaneous tissue, and skin were sutured. An antibiotic (cefazolin, 20 mg kg^{-1} subcutaneously twice daily) and an analgesic (buprenorpine, 15 μg kg^{-1} intramuscularly twice daily) were administered for 3 days after implantation. This study was conducted under the Guidelines of the Animal Care Committee of the Graduate School of Agricultural and Life Sciences, the University of Tokyo.

2.3.2. Biomechanical analysis

8 weeks after implantation the distal part of the femur was excised, and the surrounding tissue removed. The normal femur was used as the positive control ($n = 5$). The specimes was fixed with bone cement with the longitudinal axis of the bone defect vertical to the slab of a rheometer (CR-500DX, Sun Scientific Co., Japan), and a rod 5 mm in diameter was preloaded on the surface of the defect site at 1 N force. The specimen was loaded at 3 mm min^{-1}, and stopped when displacement reached a depth of 0.25 mm to avoid destruction of the specimen. Force–displacement changes in the bone defect were observed and the stiffness calculated from the slope of the linear region of the resulting force–displacement curve.

2.3.3. Histological analysis

After the biomechanical analysis the bone around the implant sites was trimmed and fixed with 10% neutralized formaldehyde

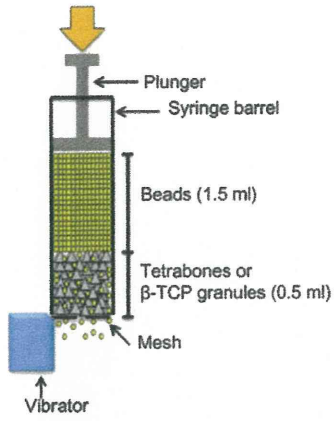

Fig. 1. A novel method of evaluating the size and connectivity of intergranular pores.

for 1 week, then demineralized with Plank-Rychlo decalcifying solution for 20 weeks. It was then embedded in paraffin, cut into 7 μm thick longitudinal sections, and stained with Masson's Trichrome.

To evaluate the new bone tissue a picture of the entire specimen was taken under a light microscope (Biozero, Keyence, Japan). The ratios of new bone area and distribution were measured using ImageJ software (National Institutes of Health, Bethesda, MD). To evaluate the new bone area we measured only the new bone tissue showing a calcified dense matrix which stained deep blue at high magnification. To evaluate the distribution the extended margins of the new bone tissue were measured, and the outer area of the margins were defined as the distribution of new bone tissue.

2.4. Statistical analysis

All data are expressed as means and standard deviations. Statistical analysis was performed using SPSS software (IBM, New York, NY). One-way analysis of variance was performed to compare the properties of Tetrabones and β-TCP granules, with Tukey's post hoc test applied for the biomechanical analysis in vivo. P values of less than 0.05 were considered statistically significant.

3. Results

3.1. Fabrication of Tetrabones

Tetrabones of homogeneous shape and size (1 mm) were fabricated by injection molding and succinic acid treatment. The macromorphology of Tetrabones was visualized by SEM, which confirmed their uniform size and shape (Fig. 2A). In contrast, β-TCP granules showed heterogeneous shapes and sizes (Fig. 2B).

3.2. Material properties of Tetrabones

3.2.1. X-ray diffraction analysis

XRD was performed to confirm OCP formation on Tetrabones by succinic acid treatment. The XRD patterns of pure α-TCP powder and the injectionmolded products before and after succinic acid treatment are shown in Fig. 3. The XRD patterns of the injectionmolded products before succinic acid treatment fitted the standard peak of α-TCP well. After succinic acid treatment the main peak observed at $2\theta = 4.70°$ was assigned to OCP, while peaks at around $2\theta = 30°$ indicated mainly TCP and other calcium phosphate complexes. These results indicate that some part of Tetrabones was recrystallized into OCP and other calcium phosphates by succinic acid treatment. The XRD of β-TCP granules showed pure β-TCP peaks.

3.2.2. Assessment of surface structure

SEM was also performed to observe the surface structure of Tetrabones. SEM of the injectionmolded products before succinic acid treatment revealed globular particles similar to pure α-TCP powder (Fig. 4A and B). After succinic acid treatment thin plate-like crystals characteristic of OCP were observed on the surface of the Tetrabones (Fig. 4C and Supplementary Fig. 1). These data suggest that α-TCP on the surface of Tetrabones was recrystallized into OCP, while the inner structure beneath the surface was mainly TCP and other calcium phosphate complexes, which may support the XRD data.

3.2.3. Mechanical testing

To assess the mechanical properties of Tetrabones and β-TCP granules the rupture strength of single granules and the elastic modulus of aggregates were evaluated using a rheometer and a universal testing machine, respectively.

The rupture strength of single Tetrabone particles was 3.45 ± 0.42 N and that of β-TCP granules was 1.20 ± 0.42 N (Fig. 5A). The elastic modulus of aggregated particles was 65.15 ± 7.98 MPa for the Tetrabones and 7.85 ± 3.43 MPa for the β-TCP granules (Fig. 5B). Both parameters were significantly higher in the Tetrabone group than in the β-TCP granule group ($P < 0.05$).

3.2.4. Analysis of size and connectivity of intergranular pores

The weights of 100 μm diameter beads passing through the Tetrabone packed or β-TCP granule packed syringes were 0.236 ± 0.030 and 0.135 ± 0.034 g, respectively ($P < 0.05$); for the 300 μm beads these weights were 0.214 ± 0.014 and 0.010 ± 0.002 g ($P < 0.05$); for the 400 μm beads they were 0.046 ± 0.011 and 0.021 ± 0.005 g ($P < 0.05$). However, the 600 μm diameter beads did not pass through either material (Fig. 6A).

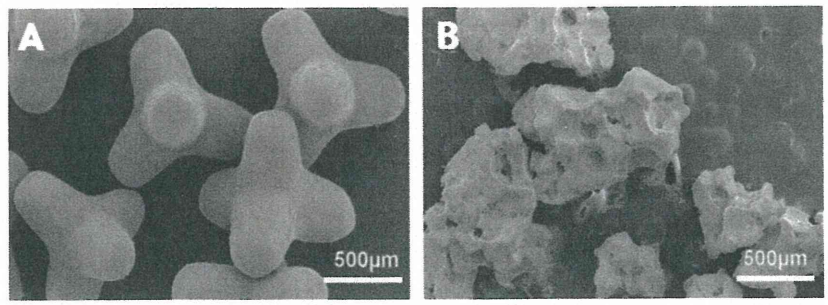

Fig. 2. Macromorphology (SEM image) of (A) Tetrabones and (B) β-TCP granules. Scale bar 500 μm.

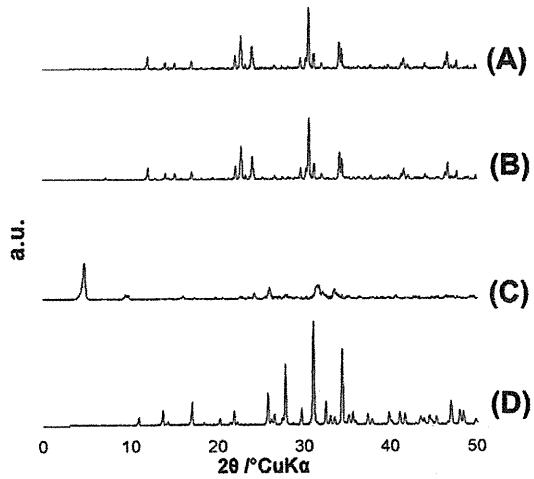

Fig. 3. XRD patterns of pure (A) α-TCP powder, injectionmolded products (B) before and (C) after succinic acid treatment (Tetrabones), and (D) β-TCP granules. The white arrowhead indicates a peak of α-TCP; the black arrowhead indicates a peak of OCP.

Thus the connectivity of the 100–400 μm intergranular pores was significantly higher in the Tetrabone group than in the β-TCP granule group, suggesting that Tetrabones have intergranular pores that may be more supportive of cell and vascular invasion than conventional artificial bone materials.

Using mercury porosimetry there were no significant differences between these values for the 100–300, 300–400 and 400–500 μm beads (Fig. 6B).

3.2.5. Cell viability

To evaluate the effect of Tetrabones on cell viability the number of cells attached to the surface of the artificial bone was counted after 7 days in culture. The number of attached cells was $17.40 \pm 1.67\ mm^{-2}$ in the Tetrabone group and $16.00 \pm 1.41\ mm^{-2}$ in the β-TCP granule group (Fig. 7), which was not significantly different. These data suggest that Tetrabones and β-TCP granules show comparable abilities to support viable attached cells.

3.3. In vivo experiments

3.3.1. Biomechanical analysis

The biomechanical properties of Tetrabones were evaluated 8 weeks after implantation in vivo, by measuring the stiffness of a canine femoral defect filled with Tetrabones or β-TCP granules. The resulting force–displacement curves for each specimen are shown in Fig. 8A. The stiffness was $27.99 \pm 5.87\ N\ mm^{-1}$ for the normal bone group, $21.59 \pm 2.43\ N\ mm^{-1}$ for the Tetrabone implantation group, $2.91 \pm 2.15\ N\ mm^{-1}$ for the β-TCP granule implantation group, and $1.41 \pm 1.91\ N\ mm^{-1}$ for the control group (Fig. 8B), respectively. The stiffness of the normal bone group was significantly higher than the other groups, and the Tetrabone implantation group was significantly higher (7.4-fold, $P < 0.05$) than those of the β-TCP granule implantation and control groups. There was no significant difference between the β-TCP granule implantation group and the control group.

3.3.2. Histological analysis

The implantation sites of the Tetrabone implanted and β-TCP granule implanted femurs were analyzed histologically for evidence of new bone growth. The surface of the Tetrabones was found to be surrounded by new bone tissue, which was present in most of the defect area (Fig. 9A). Moreover, most of the intergranular pores were filled with new bone tissue and bone marrow cells (Fig. 9D). In the β-TCP granule implantation group there was abundant new bone tissue at the margins of the defect (Fig. 9B), while most of the tissue in the central area was fibrous tissue (Fig. 9E). In the control group a large dead space without any tissue was observed in the central area (Fig. 9C), and at the marginal site most of the tissue was fibrous tissue (Fig. 9F).

The ratios of new bone area in the bone defects were 16.23 ± 2.31% in the Tetrabone implantation group, 15.78 ± 3.11% in the β-TCP granule implantation group and 6.97 ± 2.64% in the control group, respectively. Those of the Tetrabone implantation

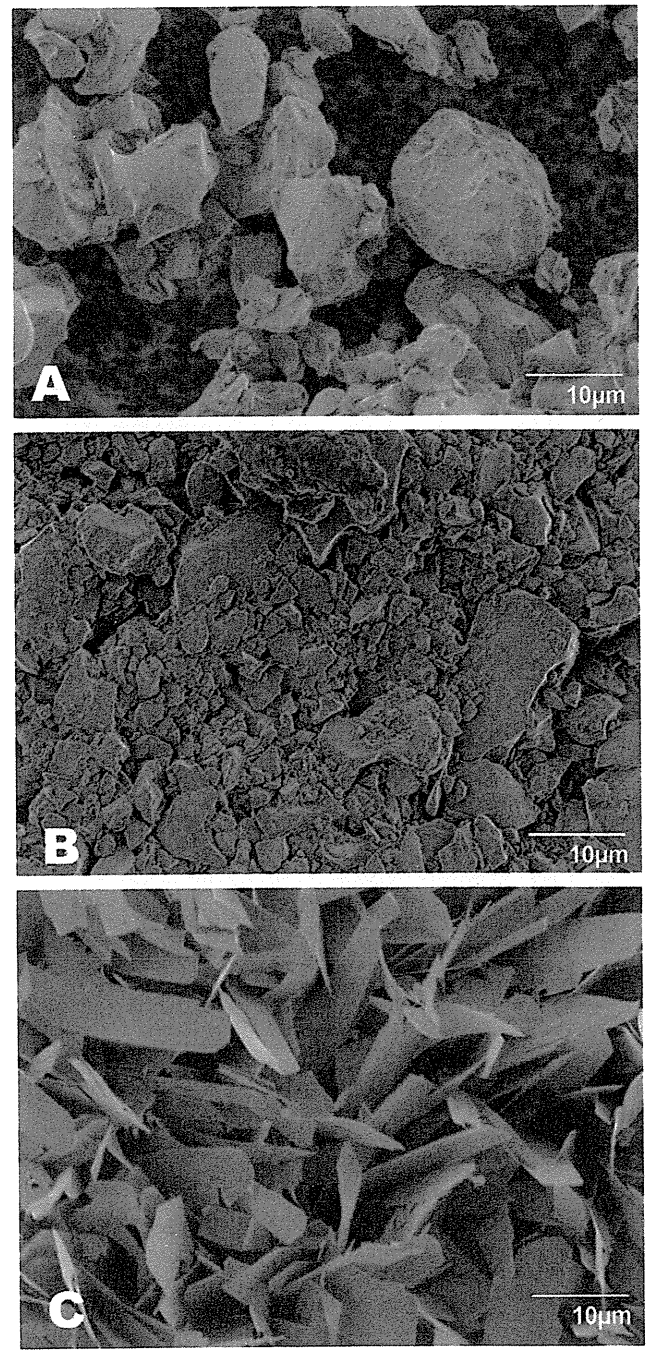

Fig. 4. SEM images of (A) pure raw α-TCP powder, injectionmolded products (B) before succinic acid treatment and (C) after succinic acid treatment (Tetrabones). Scale bar 10 μm.

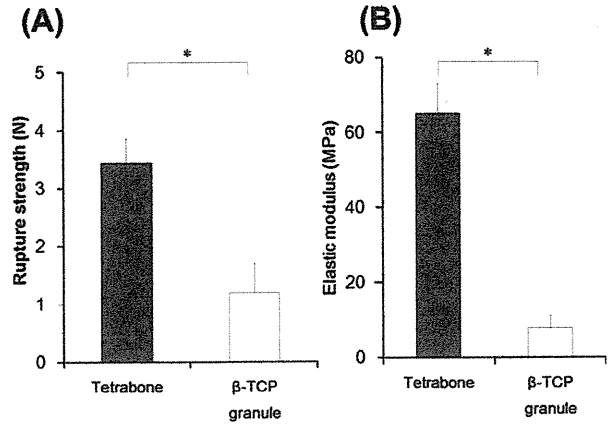

Fig. 5. Mechanical properties of Tetrabones and β-TCP granules. (A) Rupture strength of a single particle of Tetrabone and β-TCP granules and (B) the elastic modulus of assembled particles of Tetrabones and β-TCP granules. *$P < 0.05$.

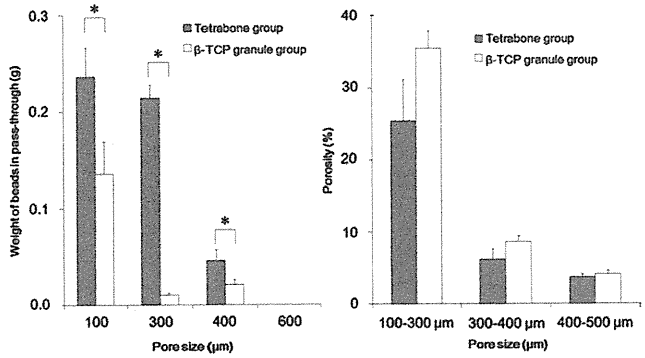

Fig. 6. Analysis of the size and connectivity of intergranular pores using (A) microbeads and (B) mercury porosimetry in the Tetrabone group and the β-TCP granule group. *$P < 0.05$.

and the β-TCP granule implantation groups were significantly higher than that of the control group ($P < 0.05$), and there was no significant difference between those of the Tetrabones and β-TCP granule implantation groups. The ratios of new bone distribution in the bone defects were 89.68 ± 7.34% in the Tetrabone implantation group, 60.87 ± 12.39% in the β-TCP granule implantation group and 44.98 ± 12.09% in the control group, respectively. Those of the Tetrabone implantation group and the β-TCP granule implantation group were significantly higher than that of the control group ($P < 0.05$), and that of the Tetrabone implantation group was significantly higher than that of the β-TCP granule implantation group ($P < 0.05$, Fig. 9G).

The Tetrabone implantation group showed a new bone area comparable with that of the β-TCP granule implantation group, and new bone tissue was homogeneously distributed in bone defects in the Tetrabone implantation group, while it was heterogeneously distributed in the β-TCP granule implantation group.

4. Discussion

Calcium phosphate granules of various shapes and sizes have been used widely in clinical practice [10–12]. However, they can only be used for non-load-bearing sites due to their poor biomechanical strength [8,13]. The four-armed tetrapod structure was designed by civil engineers to dissipate force and reduce displacement by allowing a random distribution of tetrapods to mutually

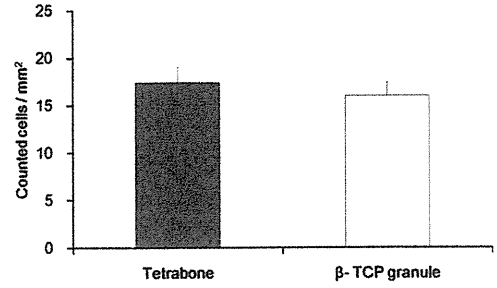

Fig. 7. Cell viability on Tetrabones and β-TCP granules. Seven days after osteogenic culture the number of MC3T3-E1 cells per square millimeter of Tetrabones or β-TCP granules was determined by ALP staining.

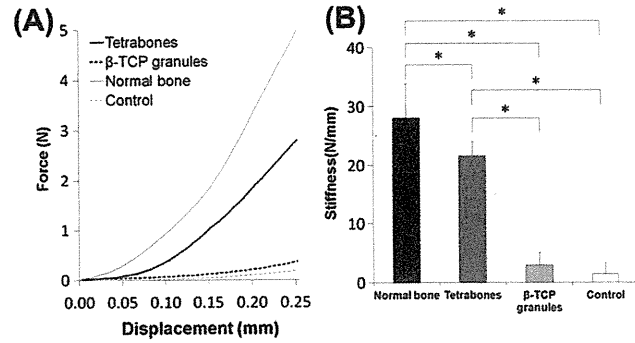

Fig. 8. Biomechanical properties of normal bone, non-treated defects and the implantation sites of Tetrabones and β-TCP granules 2 months after implantation. (A) Force–displacement curve and (B) stiffness of the bone defects. *$P < 0.05$.

interlock. We hypothesized that the same principle could be applied to artificial bone graft materials and thus developed tetrapod-shaped Tetrabones. In the present study we have evaluated their mechanical strength, their ability to retain their shape in bone defects in vivo, and the formation of intergranular pores that allow invasion by cells and blood vessels. Tetrabones showed greater mechanical strength than β-TCP granules as both single units and in aggregates, which can be attributed to both its composition and shape. First, the α-TCP crystals on the Tetrabone surface recrystallize as OCP after succinic acid treatment, which has high mechanical strength [14]. Second, as described above, the load force on accumulated Tetrabones was likely evenly dissipated due to the mechanical stability imparted by their homogeneous and symmetrical structure.

In addition to its high mechanical strength, OCP is known to have excellent biocompatibility, osteoconductivity, and biodegradability [15–17]. Our in vitro experiments with MC3T3-E1 cells under osteogenic culture conditions revealed that cells attached to OCP-coated Tetrabones had comparable viability to those attached to β-TCP granules. In a previous study OCP was shown to facilitate the differentiation of osteogenic cells into osteoblastic cells, although the mechanism by which this occurs remains unknown [18]. These characteristics likely contributed to the good osteoconductivity displayed by Tetrabones.

The size and connectivity of intergranular pores are important factors for bone regeneration because they facilitate vascular and tissue in growth [19,20]. In addition, Tamai et al. have reported that pore interconnectivity is a primary determinant of osteoconductivity [21]. We hypothesized that their homogeneous shape and size would allow accumulated Tetrabones to create more effective intergranular pores than β-TCP granules for cell and vascular invasion. We tested this hypothesis by devising a novel

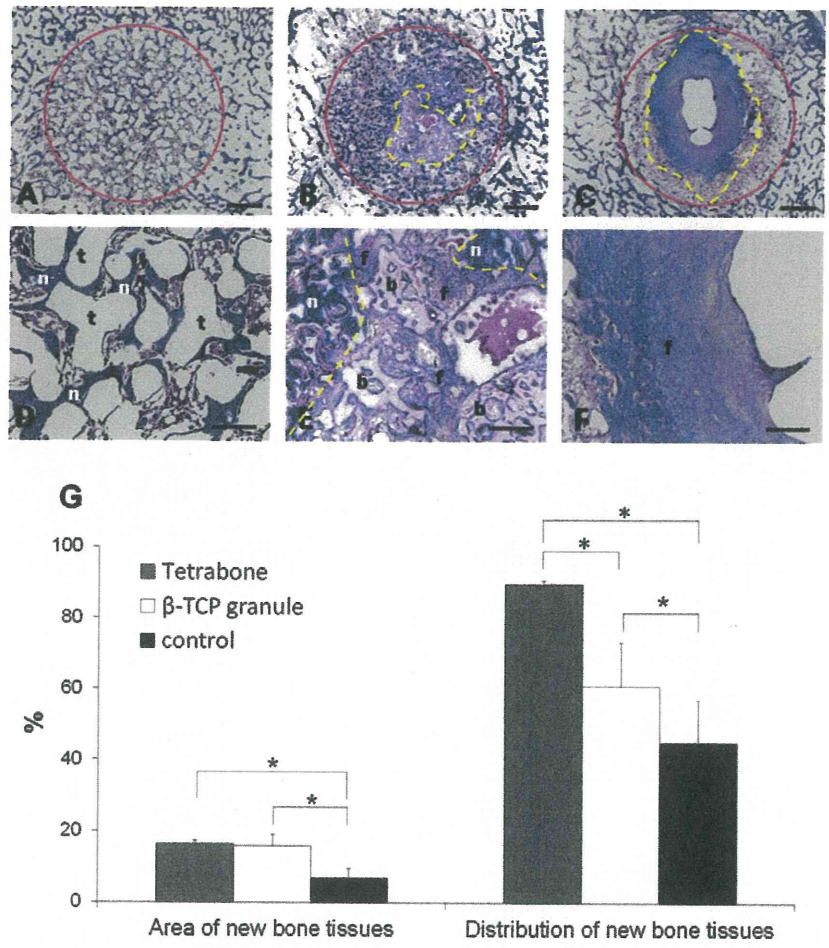

Fig. 9. Histological findings for the implantation sites of each group. Masson Trichromestaining 2 months after implantation of (A and D)Tetrabones and (B and E) β-TCP granules and (C and F) non-treated bone. *$P < 0.05$. Solid line, the bone defect; dotted line, the extended margin of new bone tissue; n, the new bone tissues; f, fibrous tissues; b, β-TCP granule; t, Tetrabone. Scale bar2 mm (A–C); 500 μm (D–F).

method using microbeads to assess the intergranular pores sizes in Tetrabones and β-TCP granules. Mercury porosimetry is a typical method to evaluate pore sizes from 0.1 to 1000 μm and has been widely used to evaluate the porous structure of various calcium phosphate materials [21,22]. However, this method is not suitable for porosity evaluation when the pore connection has a inlet that narrows or a pathway with an hourglass or ink bottle form [23,24]. If an inlet or a pathway is smaller than the diameter of a cell, although there is sufficient space beyond the inlet, the space may be accessible to mercury but inaccessible to cells and blood vessels, thus creating a "dead space" within the tissue. Mercury porosimetry may overestimate the intergranular pores by including these dead spaces. To address this problem we used a novel method to evaluate the size and connectivity of the intergranular pores using microbeads passing through Tetrabones or β-TCP granules to simulate passage of cells and blood vessels through the pores. We could evaluate the connectivity of the intergranular pores excluding those pores smaller than a certain size by this novel method. In this study, although the mercury porosimetry results indicated no significant differences between two groups, the results of the novel method using microbeads indicated higher intergranular pore connectivity in the Tetrabone group. These results using the novel method agreed with the histological findings, which showed homogeneously distributed new bone tissue in the Tetrabone implantation group and heterogeneously distributed new bone tissue in the β-TCP granule implantation group. These data suggest that this novel method using microbeads may be more appropriate to evaluate the size and connectivity of intergranular pores than mercury porosimetry. This is a simple method using microbeads and a syringe and is effective in evaluating the connectivity of intergranular pores, although this cannot measure the total porosity of the materials.

β-TCP granules, having a heterogeneous size and shape, showed fewer effective intergranular pores than did Tetrabones. It is possible that smaller β-TCP granules were situated between larger granules, thus obstructing the connection of intergranular pores. It is also known that granules with a homogeneous shape are less pro-inflammatory and facilitate faster bone in growth than granules having a heterogeneous shape [25].

Several studies have examined the pore size of calcium phosphate implants, and have reported that a pore size of about 100–1000 μm is adequate for bone regeneration [26–29], with a minimum pore size of 50 μm being recommended [30]. In the present study the accumulated Tetrabones were porous to 100, 300, and 400 but not 600 μm beads, suggesting that the intergranular pore size is less than 600 μm. Kuhne et al. reported that larger pore sizes led to higher osteoconductivity [26]. However, larger pore sizes also reduce the mechanical strength of the implant [31], suggesting that, on balance, a larger pore size is not necessarily a desirable property. There is a granular material called JAX™ (Smith and Nephew Orthopaedics Ltd.) similar to Tetrabone. JAX™ is 4 mm in diameter and made of β-TCP, and has a six-armed structure to provide 55% intergranular porosity ranging from 40 to 3000 μm. It has been reported that JAX™ has good osteoconductivity, and

has also been used as a drug delivery system in combination with osteogenic cells and anosteoinductive factor in previous studies [32,33]. However, it is limited to use for non-load-bearing defects because of its fragility [34]. In this study Tetrabone showed high mechanical strength in vitro and in vivo, suggesting potential application for load-bearing defects. Further study is needed to compare Tetrabones and JAX™ by investigating the mechanical properties, granule sizes (1 and 4 mm), number of arms (four or six), intergranular pore sizes and connections (under 600 and under 3000 μm).

β-TCP granules have been shown to have excellent osteoconductivity due to their superior biocompatibility and biodegradability in vivo [35,36]. In this study the β-TCP granule implantation group showed abundant new bone tissue in bone defects, as in previous studies. However, the new bone tissue was heterogeneously distributed. These phenomena may result from this particular bone defect model and a short observation period. In this study the observation period may not have been long enough to fully regenerate new bone tissue in the β-TCP granules implantation group. However, over a longer period some β-TCP granules might biodegrade in vivo before bone formation, and they may also lose their osteoconductive function and mechanical strength [37]. Actually, in the β-TCP granule implantation group there was less new bone tissue in the central area of the defect, with more fibrous tissue. The Tetrabone implantation group showed homogeneously distributed new bone tissue with less fibrous tissue, although the new bone area was comparable in both groups. This may indicate that Tetrabones have more connected intergranular pores. The larger connected intergranular pores of Tetrabones provide an effective scaffold, and facilitate more new bone tissue in the central area of the defects.

Several groups have performed biomechanical analyzes of the implantation site of artificial bones using bending or compression tests [38,39]. These methods are destructive and thus do not allow further evaluation of the sample. In this study we used a non-destructive method to assess biomechanical strength, which allowed subsequent histological analysis to be performed on the same samples. A similar method has been used to evaluate spine stiffness [40,41]. In an earlier preliminary study using cadaver samples we confirmed that elastic deformation was exhibited at 0.25 mm displacement without structural destruction. Therefore, we measured the stiffness up to 0.25 mm displacement. Although this method measures only stiffness, it still provides useful information to help explain the mechanical properties of the implant site.

In this study we used conventional β-TCP granules, having a heterogeneous size and shape, as the control. However, these two materials are not only different in size and shape, but also in surface structure and biodegradability due to their chemical compositions and different packing densities and surface areas when they form aggregates. Since these factors may influence the bone healing process in vivo further study should be performed taking these factors into consideration.

5. Conclusions

We succeeded in fabricating uniform 1 mm sized tetrapod shaped granular artificial bone coated with OCP, which we named Tetrabones. Tetrabones has a higher mechanical strength than conventional β-TCP granules in vitro, and, when forming aggregates, formed intergranular pores of an appropriate size and connectivity for cell and vascular invasion. Tetrabone implantation provided proper biomechanical properties to stabilize a bone defect and induce homogeneously distributed new bone tissue in vivo due to their proper intergranular pore connection after 2 months implantation. We conclude that Tetrabones have appropriate biomechanical properties and osteoconductive potential and may be a good bone graft material for bone reconstruction comparable with conventional granular artificial bone.

Acknowledgements

This research was supported by the Japan Society for the Promotion of Science through the "Funding Program for WorldLeading Innovative R&D in Science and Technology (FIRST Program)", initiated by the Council for Science and Technology Policy.

Appendix A. Supplementary data

Supplementary data associated with this article can be found, in the online version, at doi:10.1016/j.actbio.2012.02.019.

References

[1] Arrington ED, Smith WJ, Chambers HG, Bucknell AL, Davino NA. Complications of iliac crest bone graft harvesting. Clin Orthop Relat Res 1996;329:300–9.
[2] Sen MK, Miclau T. Autologous iliac crest bone graft: should it still be the gold standard for treating nonunions? Injury 2007;38(Suppl. 1):S75–80.
[3] Dorozhkin SV. Bioceramics of calcium orthophosphates. Biomaterials 2010;31(7):1465–85.
[4] Trombelli L, Heitz-Mayfield LJ, Needleman I, Moles D, Scabbia A. A systematic review of graft materials and biological agents for periodontal intraosseous defects. J Clin Periodontol 2002;29(Suppl. 3):117–35. discussion 160–112.
[5] Simpson D, Keating JF. Outcome of tibial plateau fractures managed with calcium phosphate cement. Injury 2004;35(9):913–8.
[6] Nair MB, Varma HK, Menon KV, Shenoy SJ, John A. Reconstruction of goat femur segmental defects using triphasic ceramic-coated hydroxyapatite in combination with autologous cells and platelet-rich plasma. Acta Biomater 2009;5(5):1742–55.
[7] Sopyan I, Mel M, Ramesh S, HKhalid KA. Porous hydroxyapatite for artificial bone applications. Sci Tech Adv Mater 2007;8:116–23.
[8] Costantino PD, Friedman CD, Jones K, Chow LC, Sisson GA. Experimental hydroxyapatite cement cranioplasty. Plast Reconstr Surg 1992;90(2):174–85. discussion 186–191.
[9] Franco L, Noli A, Paolo DG, Ercolani M. Concrete strength and durability of prototype tetrapods and dolosse: results of field and laboratory tests. Coast Eng 2000;40(3):207–19.
[10] Komuro Y. Use of calcium phosphate cement in craniofacial surgery. Med Postgraduates 2003;41(2):36–40.
[11] Garrido CA, Lobo SE, Turibio FM, Legeros RZ. Biphasic calcium phosphate bioceramics for orthopaedic reconstructions: clinical outcomes. Int J Biomaterials 2011;2011:129727.
[12] Chawla K, Lamba AK, Faraz F, Tandon S. Evaluation of beta-tricalcium phosphate in human infrabony periodontal osseous defects: a clinical study. Quintessence Int 2011;42(4):291–300.
[13] Linhart W, Briem D, Amling M, Rueger JM, Windolf J. Mechanical failure of porous hydroxyapatite ceramics 7.5 years after implantation in the proximal tibia. Unfallchirurg 2004;107(2):154–7.
[14] Komlev VS, Fadeeva IV, Barinov SM, Rau JV, Fosca M, Gurin AN, et al. Phase development during setting and hardening of a bone cement based on {alpha}-tricalcium- and octa calcium phosphates. J Biomater Appl. 2011. doi:10.1177/0885328210390403 [Epub ahead of print].
[15] Kamakura S, Sasano Y, Homma H, Suzuki O, Kagayama M, Motegi K. Implantation of octacalcium phosphate nucleates isolated bone formation in rat skull defects. Oral Dis 2001;7(4):259–65.
[16] Oonishi H, Hench LL, Wilson J, Sugihara F, Tsuji E, Kushitani S, et al. Comparative bone growth behavior in granules of bioceramic materials of various sizes. J Biomed Mater Res 1999;44(1):31–43.
[17] Chow LC. Next generation calcium phosphate-based biomaterials. Dent Mater J 2009;28(1):1–10.
[18] Suzuki O, Kamakura S, Katagiri T, Nakamura M, Zhao B, Honda Y, et al. Bone formation enhanced by implanted octacalcium phosphate involving conversion into Ca-deficient hydroxyapatite. Biomaterials 2006;27(13):2671–81.
[19] Eggli PS, Muller W, Schenk RK. Porous hydroxyapatite and tricalcium phosphate cylinders with two different pore size ranges implanted in the cancellous bone of rabbits. A comparative histomorphometric and histologic study of bony in growth and implant substitution. Clin Orthop Relat Res 1988;232:127–38.
[20] Ghanaati S, Barbeck M, Orth C, Willershausen I, Thimm BW, Hoffmann C, et al. Influence of beta-tricalcium phosphate granule size and morphology on tissue reaction in vivo. Acta Biomater 2010;6(12):4476–87.
[21] Tamai N, Myoui A, Tomita T, Nakase T, Tanaka J, Ochi T, et al. Novel hydroxyapatite ceramics with an interconnective porous structure exhibit superior osteo conduction in vivo. J Biomed Mater Res 2002;59(1):110–7.

[22] Kasten P, Beyen I, Niemeyer P, Luginbuhl R, Bohner M, Richter W. Porosity and pore size of beta-tricalcium phosphate scaffold can influence protein production and osteogenic differentiation of human mesenchymal stem cells: an in vitro and in vivo study. Acta Biomater 2008;4(6):1904–15.
[23] Yoshida R, Kishi T. Proposed approach of determination of pore continuity and suitable intrusion pressure based on step-by-step mercury intrusion porosimetery test. Seisankenkyu 2008;60(5):516–9.
[24] Diamond S. Mercury porosimetry an inappropriate method for the measurement of pore size distributions in cement-based materials. Cement Concrete Res 2000;30:1517–25.
[25] Paul W, Sharma CP. Development of porous spherical hydroxyapatite granules: application towards protein delivery. J Mater Sci Mater Med 1999;10(7): 383–8.
[26] Kuhne JH, Bartl R, Frisch B, Hammer C, Jansson V, Zimmer M. Bone formation in coralline hydroxyapatite. Effects of pore size studied in rabbits. Acta Orthop Scand 1994;65(3):246–52.
[27] Flautre B, Descamps M, Delecourt C, Blary MC, Hardouin P. Porous HA ceramic for bone replacement: role of the pores and interconnections – experimental study in the rabbit. J Mater Sci Mater Med 2001;12(8):679–82.
[28] Flatley TJ, Lynch KL, Benson M. Tissue response to implants of calcium phosphate ceramic in the rabbit spine. Clin Orthop Relat Res 1983;179 :246–52.
[29] Sanchez-Sálcedo S, Arcos D, Vallet-Regí M. Upgrading calcium phosphate scaffolds for tissue engineering applications. Key Eng Mater 2008;3777:19–42.
[30] Chang BS, Lee CK, Hong KS, Youn HJ, Ryu HS, Chung SS, et al. Osteoconduction at porous hydroxyapatite with various pore configurations. Biomaterials 2000;21(12):1291–8.
[31] Xu HH, Quinn JB, Takagi S, Chow LC, Eichmiller FC. Strong and macroporous calcium phosphate cement: effects of porosity and fiber reinforcement on mechanical properties. J Biomed Mater Res 2001;57(3):457–66.
[32] Clarke SA, Hoskins NL, Jordan GR, Henderson SA, Marsh DR. In vitro testing of Advanced JAX Bone Void Filler System: species differences in the response of bone marrow stromal cells to beta tri-calcium phosphate and carboxymethylcellulose gel. J Mater Sci Mater Med 2007;18(12): 2283–90.
[33] Clarke SA, Hoskins NL, Jordan GR, Marsh DR. Healing of an ulnar defect using a proprietary TCP bone graft substitute, JAX, in association with autologous osteogenic cells and growth factors. Bone 2007;40(4):939–47.
[34] Field JR, McGee M, Wildenauer C, Kurmis A, Margerrison E. The utilization of a synthetic bone void filler (JAX) in the repair of a femoral segmental defect. Vet Comp Orthop Traumatol 2009;22(2):87–95.
[35] Komaki H, Tanaka T, Chazono M, Kikuchi T. Repair of segmental bone defects in rabbit tibiae using a complex of beta-tricalcium phosphate, type I collagen, and fibroblast growth factor-2. Biomaterials 2006;27(29): 5118–26.
[36] Moore WR, Graves SE, Bain GI. Synthetic bone graft substitutes. Aust N Z J Surg 2001;71(6):354–61.
[37] Murakami Y, Honda Y, Anada T, Shimauchi H, Suzuki O. Comparative study on bone regeneration by synthetic octacalcium phosphate with various granule sizes. Acta Biomater 2010;6(4):1542–8.
[38] Zhang C, Wang J, Feng H, Lu B, Song Z, Zhang X. Replacement of segmental bone defects using porous bioceramic cylinders: a biomechanical and X-ray diffraction study. J Biomed Mater Res 2001;54(3):407–11.
[39] Chang RC, Kao AS. Biomechanical and histological studies of particulate hydroxylapatite implanted in femur bone defects of adult dogs. Int J Oral Maxillofac Surg 2000;29(1):54–61.
[40] Shirley D, Ellis E, Lee M. The response of posteroanterior lumbar stiffness to repeated loading. Man Ther 2002;7(1):19–25.
[41] Snodgrass SJ, Rivett DA, Robertson VJ. Measuring the posteroanterior stiffness of the cervical spine. Man Ther 2008;13(6):520–8.

FULL PAPER *Surgery*

Effect of Trehalose Coating on Basic Fibroblast Growth Factor Release from Tailor-Made Bone Implants

Sungjin CHOI[1]*, Jongil LEE[1], Kazuyo IGAWA[2], Shigeki SUZUKI[3], Manabu MOCHIZUKI[1], Ryohei NISHIMURA[1], Ung-il CHUNG[2] and Nobuo SASAKI[1]

[1]*Laboratory of Veterinary Surgery, Graduate School of Agricultural and Life Sciences, The University of Tokyo, 1–1–1 Yayoi, Bunkyo-ku, Tokyo 113–8657,* [2]*Division of Tissue Engineering, University of Tokyo Hospital, 7–3–1 Hongo, Bunkyo-ku, Tokyo 113–0033 and* [3]*NEXT21 K.K., 3–38–1, Hongo, Bunkyo-ku, Tokyo 113–0033, Japan*

(Received 13 January 2011/Accepted 6 July 2011/Published online in J-STAGE 20 July 2011)

ABSTRACT. Artificial bone implants are often incorporated with osteoinductive factors to facilitate early bone regeneration. Calcium phosphate, the main component in artificial bone implants, strongly binds these factors, and in a few cases, the incorporated proteins are not released from the implant under conditions of physiological pH, thereby leading to reduction in their osteoinductivity. In this study, we coated tailor-made bone implants with trehalose to facilitate the release of basic fibroblast growth factor (bFGF). In an *in vitro* study, mouse osteoblastic cells were separately cultured for 48 hr in a medium with a untreated implant (T–), trehalose-coated implant (T+), bFGF-incorporated implant (FT–), and bFGF-incorporated implant with trehalose coating (FT+). In the FT+ group, cell viability was significantly higher than that in the other groups ($P<0.05$). Scanning electron microscopy (SEM) and X-ray diffraction (XRD) revealed that trehalose effectively covered the surface of the artificial bone implant without affecting the crystallinity or the mechanical strength of the artificial bone implant. These results suggest that coating artificial bone implants with trehalose could limit the binding of bFGF to calcium phosphate.

KEY WORDS: artificial bone implant, bFGF, *in vitro*, trehalose.

J. Vet. Med. Sci. 73(12): 1547–1552, 2011

Tailor-made bone implants fabricated from α-tricalcium phosphate (α-TCP; $[Ca_3(PO_4)_2]$) by using inkjet 3D biofabrication technology showed excellent osteoconductivity in dogs with bone defects [4, 10]. These implants were designed to match the shape of the bone defect. In addition, the internal structures of the implants, such as cylindrical holes, were freely designed to improve the osseointegration. However, these tailor-made implants had only osteoconductivity, and not osteoinductivity. Osteoconductive bone implants require substantial amount of time to stabilize, thereby causing slow bone regeneration. Therefore, various studies are being conducted to increase the regenerative capability of implants by incorporating various osteoinductive factors in these implants [8, 9, 21].

Osteoinductive molecules such as bone morphogenetic protein (BMP) and basic fibroblast growth factor (bFGF) can induce differentiation and proliferation of osteoblastic cells [2, 13, 34, 35]. However, these molecules need appropriate carriers to maintain their biological activity because of the short half-life of the molecules *in vivo*. Drug delivery systems (DDSs) used as carriers of osteoinductive molecules should incorporate and store drug molecules and release them during a suitable phase without inactivating the molecules. Calcium phosphates are among the DDSs used as carriers for osteoinductive molecules because of the self-setting ability, injectability, and biodegradability of calcium phosphates [7, 8]. Furthermore, calcium phosphate has a greater affinity for the incorporated protein than that shown by most other materials that are used as carriers [30]. In some cases, calcium phosphate may show very high affinity for the incorporated proteins, thereby preventing the release of the proteins [20]. At times, the incorporated proteins may not be released from the calcium phosphate under conditions of physiological pH, leading to a reduction in their function [19]. These findings suggest that bFGF incorporated into tailor-made bone implants made of α-TCP may not be released at an appropriate time to induce bone regeneration.

Trehalose is a non-reducing disaccharide found in a wide variety of living organisms such as fungi, plants, and animals. Although the mechanism underlying the cell-protective function of trehalose remains unclear, trehalose can protect the cells from a variety of environmental stresses such as desiccation, dehydration, freezing, and oxidation [3, 6, 26]. Because of these protective effects of trehalose in living systems, it is widely used in food, cosmetics, and drugs. We hypothesized that coating of the artificial bones with trehalose may prevent strong incorporation of bFGF in α-TCP.

One concern related to trehalose coating of artificial bone implants is that the coating may reduce the mechanical strength of the artificial bone. This concern is attributable to the fact that tailor-made implants appeared more fragile after being soaked in water. If trehalose solution is used to coat artificial bones, they may become fragile, which in turn may decrease the value of artificial bone implants in clinical practice. Furthermore, the detailed structures and mechani-

* CORRESPONDENCE TO: CHOI, S., Laboratory of Veterinary Surgery, Graduate School of Agricultural and Life Sciences, The University of Tokyo, 1–1–1 Yayoi, Bunkyo-ku, Tokyo 113–8657, Japan.
e-mail: tjdwls1101@hotmail.com

cal strength of trehalose-coated and non-trehalose-coated artificial implants are yet to be elucidated.

In this study, we conducted an *in vitro* study to confirm whether trehalose can prevent strong binding of bFGF by the artificial bone and allow its release from the implant at an appropriate time.

We also analyzed the microstructure, quality, and mechanical strength of the artificial bone and the resultant changes after trehalose coating.

MATERIALS AND METHODS

Preparation of implants: *Implant fabrication.* The artificial bone was fabricated according to the procedure described in previous reports [4, 10]. In brief, tailor-made implants for each experiment were designed on the basis of 3D images of the defect cavity by using the Mimics program (Materialise, Leuven, Belgium) and fabricated using a 3D inkjet printer (Z406 3D color printer; Z-corporation, Burlington, MA, U.S.A.). A liquid binder was injected from the inkjet head into a powder layer 0.1-mm in thickness to mould the powder into the desired shape. The use of liquid binder resulted in hardening of the powder material on the flat surface, and a solid figure was formed. The powder used was α-TCP (Biopex; Mitsubishi Materials, Tokyo, Japan) with a mean particle diameter of 10 μm. The liquid binder was a mixture of 5% sodium chondroitin sulfate (Seikagaku, Tokyo, Japan), 12% disodium succinate (Wako, Tokyo, Japan), and 83% distilled water (Otsuka Pharmaceuticals, Tokyo, Japan). Each hardened sheet was piled repeatedly, and artificial bone of the desired shape was produced (Fig. 1).

Trehalose coating. Trehalose was purchased from Hayashibara Corporation (Okayama, Japan). For trehalose coating, the fabricated implants were immersed overnight in 5% trehalose solution at room temperature. Then, the implants were washed with distilled water and autoclaved at 121°C for 30 min. Finally, the implants were dried under air pressure.

bFGF incorporation. bFGF was purchased from Kaken Pharmaceuticals (Tokyo, Japan) and diluted using deionized water in 1 μg/μl solution. Immediately before the experiment, the bFGF solution was dropped onto the implants with or without trehalose coating by using a micropipette; then, the implants were dried for 10 min at room temperature.

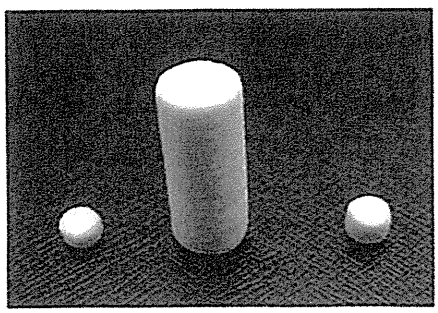

Fig. 1. Fabricated tailor-made implants for cell proliferation test (left), 3-point bending test (middle), and compression strength test (right).

Effect of bFGF incorporation in the artificial bone on in vitro cell proliferation: Disk-shaped artificial bone implants (diameter, 4 mm; height, 2 mm) were prepared for investigating cell proliferation. The implants were divided into the following 4 groups (3 implants in each group): implants without trehalose-coating (T−), implants with trehalose coating (T+), bFGF-incorporated implants (FT−), and bFGF-incorporated implants with trehalose coating (FT+).

Mouse osteoblastic cells (MC3T3-E1) were used for this study. The cells were cultured in Dulbecco's modified Eagle's medium (DMEM; Gibco, Grand Island, NY, U.S.A.) supplemented with 10% fetal bovine serum (FBS; Gibco), 200 mg/ml penicillin (Gibco), and 200 mg/ml streptomycin (Gibco) at 37°C in a humidified atmosphere of 5% CO_2. These cells were seeded in a 96-well plate at a density of 5,000 cells/well and incubated for 24 hr. The implants of all types were placed in the cell insert. The cells of all groups were incubated for 48 hr, and then, the number of viable cells was measured by using a Cell Counting Kit-8 solution (Dojindo, Kumamoto, Japan).

Scanning electron microscopy (SEM): SEM was used to observe the structure and superficial morphology of the trehalose-coated implants and non-trehalose-coated implants. The implants were lyophilized and observed using SEM (JCM-5700; JEOL, Tokyo, Japan) at an accelerating voltage of 1.2 kV.

X-ray diffraction (XRD) for qualitative analysis: An X-ray diffractometer (Miniflex II; Rigaku, Tokyo, Japan) was used to assess the crystallinity of the trehalose-coated implants and non-trehalose-coated implants. The X-ray source was Cu Kα radiation, and XRD was performed at 30 kV and 15 mA with a scanning speed of 2°/min. The diffraction patterns were indexed according to the structural data in the International Centre for Diffraction Data (ICDD) Powder Diffraction File.

Mechanical strength: Strength test was performed using INSTRON universal testing machine (Instron-3365; Instron Corporation, Norwood, MA, U.S.A.) with a load cell of 5 kN and load speed of 1.0 mm/min.

Implants with a diameter of 7 mm and height of 17 mm were prepared to evaluate the maximum compression load strength. Each implant was soaked overnight in 5% trehalose solution (n=8) or 0.9% saline (n=8), washed with distilled water, and autoclaved at 121°C for 30 min. Implants that were not subjected to these treatments were used as controls (n=8).

Maximum compression load strength was calculated using the following formula:

$$\textit{Maximum compression load strength} = \frac{4N}{\pi r^2}$$

(N: load; r: diameter of the implant)

Another implant with a diameter of 4 mm and height of 3

mm was used to evaluate 3-point bending strength. The maximum 3-point bending load strength was calculated using the following formula:

$$Maximum\ bending\ load\ strength = \frac{30 \times 3N}{2rh^2}$$

(N: load; r: diameter of the implant; h: height of the implant)

Statistical analysis: For the data on cell proliferation and mechanical strength, one-way analysis of variance was performed followed by Tukey's test. A P value less than 0.05 was considered statistically significant.

RESULTS

Cell proliferation in vitro: Figure 2 shows the cell growth rate for each group. The cell growth rates in the T–, T+, and FT– groups were not significantly different, while that in the FT+ group was significantly higher than those in the other groups ($P<0.05$).

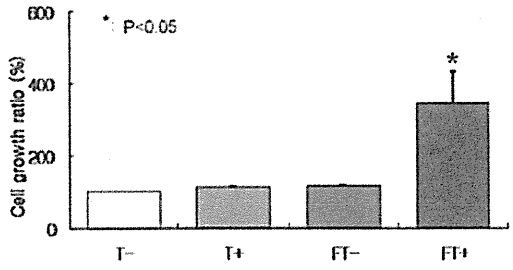

Fig. 2. Cell growth rate in each group. Trehalose-coated basic fibroblast growth factor (bFGF)-incorporated implants (FT+) show significantly higher cell proliferation rate than those observed in the other groups. T-: non-treated implants; T+: trehalose-coated implants; FT-: bFGF-incorporated implants; FT+: bFGF-incorporated implants with trehalose coating.

SEM: Figure 3 shows SEM images of T+ and T– implants. SEM images of T– implants showed microporous structures (Fig. 2A). The trehalose crystal was typically spindle-shaped due to the presence of hydroxyapatite [$Ca_{10}(PO_4)_6(OH)_2$] crystals of various sizes. SEM images of T+ implants showed that trehalose crystals covered the surface, and the crystallinity of hydroxyapatite was not completely altered by the trehalose treatment (Fig. 2B).

XRD pattern: The XRD patterns of the T+ or T– implants are shown in Fig. 4. In the T– group, the detected diffraction peaks coincided with the corresponding peaks for hydroxyapatite and α-TCP in all specimens. Additional peaks were detected because of other calcium phosphate components. No differences were detected between the diffraction patterns of T+ and T– implants.

Mechanical strength: The results of the mechanical strength test are shown in Table 1.

The bending strength and compression strength of the implants treated with saline were significantly lower than the corresponding values for T+ implants and controls ($P<0.05$). No significant differences were detected between the controls and the T+ implants with regard to bending strength and compression strength.

DISCUSSION

Various types of bone implants incorporated with bone growth factors have been reported [14, 31]. Although calcium phosphate is a good DDS, its capability to release growth factors may be poorer than that observed in other artificial bone materials [20]. Generally, the growth factor release rate of the DDS depends on the crystallinity of calcium phosphate, sinter temperature, Ca^{2+} ion affinity, and pH of the environment surrounding the bone implants [19, 27, 32, 36]. Dong *et al.* reported that BMPs bind to the -OH, $-NH_2$, and -COO- groups of hydroxyapatite, and that the Coulomb forces involved in these interactions and hydrogen bonding may affect the release of BMPs from the implant

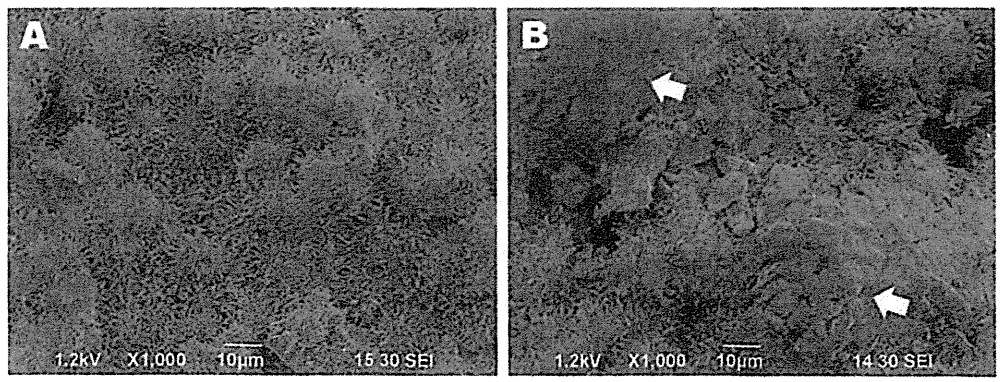

Fig. 3. Scanning electron microscopy (SEM) images of the T- and T+ implants. The surface of the T- implant is microporous and shows spindle-shaped crystals (A). The surface of the T+ implant is covered with trehalose crystals (white arrows), and the structure of the spindle-shaped crystal is maintained (B). T-: non-treated; T+: trehalose-coated.

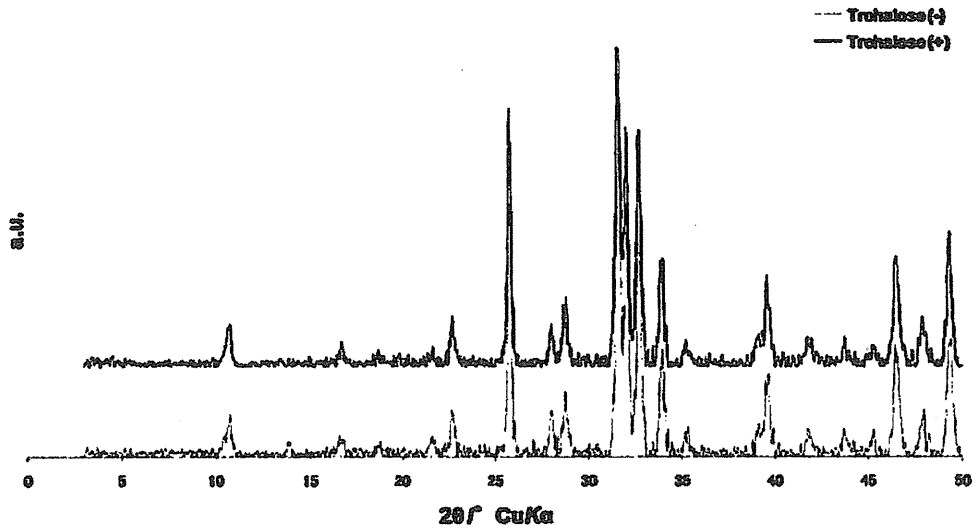

Fig. 4. X-ray diffraction patterns. X-ray diffraction patterns of the T- implants show typical patterns of hydroxyapatite and α-TCP. No difference is observed in the X-ray diffraction patterns of the T- and T+ implants. T-: non-treated; T+: trehalose-coated.

Table 1. Maximum bending and compression load strengths of each implant (unit: MPa)

	Bending strength	Compression strength
Control	6.72 ± 1.68	12.80 ± 1.28
Implants treated with trehalose	6.74 ± 1.55	13.79 ± 1.53
Implants treated with saline	5.49 ± 0.89*	9.10 ± 1.48*

Strength of the saline-treated implant was significantly lower than that of the trehalose-treated and control implants (*: $P<0.05$).

[5]. However, the binding affinity of bFGF to calcium phosphate has not yet been clarified. Onuma *et al.* reported that the binding affinity of bFGF to calcium phosphate depends on the pH and presence of NaCl [25]. However, little information is available on the release of bFGF from calcium phosphate implants. The release of bFGF from calcium phosphate crystals is difficult under conditions of physiological pH [19, 24].

In this study, we performed just cell proliferation test, but not other biologic function of bFGF such like Alkaline phosphatase activity and calcification test, because an our previous examination demonstrated the osteogenesis in canine skull (the data not shown). We hypothesized that bFGF may not be released from the calcium phosphate implants at an appropriate time. In fact, no significant increase was observed in the cell growth rate in the FT– implants compared to that in the implants without incorporation of bFGF (T+ and T– implants). The viability of the cells cultured with FT+ implants was significantly higher than that of the cells cultured with the FT– implants. These results suggest that trehalose inhibited the binding of bFGF to calcium phosphate, thereby enabling increased bFGF release. No difference was observed in the viability of the cells cultured with the T– and T+ implants, which suggests that trehalose did not affect osteoblastic cell proliferation.

Various mechanisms underlying trehalose activity have been suggested, such as stabilization of the cell membrane through hydrogen bonding, vitrification, and switching-off capability [22, 29, 33]. SEM and XRD revealed that trehalose effectively covered the surface of the implant without changing its crystallinity and basic characteristics, probably by inhibiting the binding of bFGF to calcium phosphate.

Although we used only α-TCP powder to make the implant, XRD revealed peaks of hydroxyapatite and α-TCP. A considerable change in calcium phosphate crystallinity was caused by the sinter temperature and pressure, chemical responses, and environmental hydrogen ion concentrations because of electrolytic instability. Calcium phosphates are a stable form of hydroxyapatite [28]. In this experiment, α-TCP was dissolved in the binding solution during the fabrication process of the implants. α-TCP may release Ca^{2+} and PO_4^{3-} ions into the binding solution, and then, the solution may become supersaturated with apatite, thereby leading to the formation of spindle-shaped crystals of hydroxyapatite [11, 12, 23]. This phenomenon may explain the significant presence of hydroxyapatite peaks in the XRD patterns.

When bFGF is released from calcium phosphate, bFGF may undergo degradation and its bioactivity may decrease [36]. In this study, the bFGF released from the trehalose-coated implants significantly stimulated the proliferation of osteoblastic cells, raising the following 2 hypotheses. First, trehalose may prevent the degradation of the released bFGF by binding to the bFGF protein and preserving its structure [16]. Le Nihouannen *et al.* reported that trehalose could stabilize the bioactivity of proteins bound to calcium phosphate [15]. Second, biodegradation may not decrease the bioactivity of bFGF. bFGF incorporated into the calcium phosphate implant retained substantial bioactivity [1, 18].

One of the problems associated with calcium phosphate implants is that they become fragile when soaked with the body fluids or blood, and this fragility may be attributable to the dissolution of Ca^{2+} ions into the surrounding solution [17]. In this study, the bending and compression strengths of the implants soaked with 0.9% saline were significantly lower than the corresponding values for the controls, while the mechanical strength of the implants coated with trehalose did not decrease. This finding suggests that trehalose inhibited the dissolution of Ca^{2+} ions from the implant.

In conclusion, trehalose coating of tailor-made implants could limit the binding of bFGF to calcium phosphate, facilitating the release of bFGF to induce the proliferation of osteogenic cells. Trehalose coating also prevented the decrease in mechanical strength of the implant, probably by suppressing of the dissolution of Ca^{2+} ions from the implants.

ACKNOWLEDGMENTS. This research is supported by the Japan Society for the Promotion of Science (JSPS) through its "Funding Program for World-Leading Innovative R&D on Science and Technology (FIRST Program)".

REFERENCES

1. Alam, S., Ueki, K., Marukawa, K., Ohara, T., Hase, T., Takazakura, D. and Nakagawa, K. 2007. Expression of bone morphogenetic protein 2 and fibroblast growth factor 2 during bone regeneration using different implant materials as an onlay bone graft in rabbit mandibles. *Oral Surg. Oral Med. Oral Pathol. Oral Radiol. Endod.* **103**: 16–26.
2. Canalis, E., Economides, A. N. and Gazzerro, E. 2003. Bone morphogenetic proteins, their antagonists, and the skeleton. *Endocr. Rev.* **24**: 218–235.
3. Chen, Q. and Haddad, G. G. 2004. Role of trehalose phosphate synthase and trehalose during hypoxia: from flies to mammals. *J. Exp. Biol.* **207**: 3125–3129.
4. Choi, S. J., Lee, J. I., Igawa, K., Sugimori, O., Suzuki, S., Mochizuki, M., Nishimura, R., Chung, U. I. and Sasaki, N. 2009. Bone regeneration within a tailor-made tricalcium phosphate bone implant with both horizontal and vertical cylindrical holes transplanted into the skull of dogs. *J. Artif. Organs* **12**: 274–277.
5. Dong, X., Wang, Q., Wu, T. and Pan, H. 2007. Understanding adsorption-desorption dynamics of BMP-2 on hydroxyapatite (001) surface. *Biophys. J.* **93**: 750–759.
6. Elbein, A. D., Pan, Y. T., Pastuszak, I. and Carroll, D. 2003. New insights on trehalose: a multifunctional molecule. *Glycobiology* **13**: 17R–27R.
7. Ginebra, M. P., Traykova, T. and Planell, J. A. 2006. Calcium phosphate cements as bone drug delivery systems: a review. *J. Control. Release* **113**: 102–110.
8. Habraken, W. J., Wolke, J. G. and Jansen, J. A. 2007. Ceramic composites as matrices and scaffolds for drug delivery in tissue engineering. *Adv. Drug Deliv. Rev.* **59**: 234–248.
9. Hutmacher, D. W. and Cool, S. 2007. Concepts of scaffold-based tissue engineering--the rationale to use solid free-form fabrication techniques. *J. Cell Mol. Med.* **11**: 654–669.
10. Igawa, K., Mochizuki, M., Sugimori, O., Shimizu, K., Yamazawa, K., Kawaguchi, H., Nakamura, K., Takato, T., Nishimura, R., Suzuki, S., Anzai, M., Chung, U. I. and Sasaki, N. 2006. Tailor-made tricalcium phosphate bone implant directly fabricated by a three-dimensional ink-jet printer. *J. Artif. Organs* **9**: 234–240.
11. Ishikawa, K. and Asaoka, K. 1995. Estimation of ideal mechanical strength and critical porosity of calcium phosphate cement. *J. Biomed. Mater. Res.* **29**: 1537–1543.
12. Ishikawa, K., Takagi, S., Chow, L. and Ishikawa, Y. 1995. Properties and mechanisms of fast-setting calcium phosphate cements. *J. Mater. Sci. Mater. Med.* **6**: 528–533.
13. Kawaguchi, H. 2005. Stimulation of fracture healing by FGFs. *Nippon Rinsho* **63**: 509–513 (in Japanese).
14. Komaki, H., Tanaka, T., Chazono, M. and Kikuchi, T. 2006. Repair of segmental bone defects in rabbit tibiae using a complex of beta-tricalcium phosphate, type I collagen, and fibroblast growth factor-2. *Biomaterials* **27**: 5118–5126.
15. Le Nihouannen, D., Komarova, S. V., Gbureck, U. and Barralet, J. E. 2008. Bioactivity of bone resorptive factor loaded on osteoconductive matrices: stability post-dehydration. *Eur. J. Pharm. Biopharm.* **70**: 813–818.
16. Liao, Y. H., Brown, M. B., Nazir, T., Quader, A. and Martin, G. P. 2002. Effects of sucrose and trehalose on the preservation of the native structure of spray-dried lysozyme. *Pharm. Res.* **19**: 1847–1853.
17. Liu, Y., Hunziker, E. B., Randall, N. X., de Groot, K. and Layrolle, P. 2003. Proteins incorporated into biomimetically prepared calcium phosphate coatings modulate their mechanical strength and dissolution rate. *Biomaterials* **24**: 65–70.
18. Martin, I., Muraglia, A., Campanile, G., Cancedda, R. and Quarto, R. 1997. Fibroblast growth factor-2 supports ex vivo expansion and maintenance of osteogenic precursors from human bone marrow. *Endocrinology* **138**: 4456–4462.
19. Matsumoto, T., Okazaki, M., Inoue, M., Yamaguchi, S., Kusunose, T., Toyonaga, T., Hamada, Y. and Takahashi, J. 2004. Hydroxyapatite particles as a controlled release carrier of protein. *Biomaterials* **25**: 3807–3812.
20. Midy, V., Rey, C., Bres, E. and Dard, M. 1998. Basic fibroblast growth factor adsorption and release properties of calcium phosphate. *J. Biomed. Mater. Res.* **41**: 405–411.
21. Milovancev, M., Muir, P., Manley, P. A., Seecherman, H. J. and Schaefer, S. 2007. Clinical application of recombinant human bone morphogenetic protein-2 in 4 dogs. *Vet. Surg.* **36**: 132–140.
22. Minutoli, L., Altavilla, D., Bitto, A., Polito, F., Bellocco, E., Lagana, G., Fiumara, T., Magazu, S., Migliardo, F., Venuti, F. S. and Squadrito, F. 2008. Trehalose: a biophysics approach to modulate the inflammatory response during endotoxic shock. *Eur. J. Pharmacol.* **589**: 272–280.
23. Miyamoto, Y., Ishikawa, K., Fukao, H., Sawada, M., Nagayama, M., Kon, M. and Asaoka, K. 1995. In vivo setting

behaviour of fast-setting calcium phosphate cement. *Biomaterials* **16**: 855–860.
24. Niedhart, C., Maus, U., Miltner, O., Graber, H. G., Niethard, F. U. and Siebert, C. H. 2004. The effect of basic fibroblast growth factor on bone regeneration when released from a novel in situ setting tricalcium phosphate cement. *J. Biomed. Mater. Res. A* **69**: 680–685.
25. Onuma, K., Kanzaki, N. and Kobayashi, N. 2004. Association of calcium phosphate and fibroblast growth factor-2: a dynamic light scattering study. *Macromol. Biosci.* **4**: 39–46.
26. Richards, A. B., Krakowka, S., Dexter, L. B., Schmid, H., Wolterbeek, A. P., Waalkens-Berendsen, D. H., Shigoyuki, A. and Kurimoto, M. 2002. Trehalose: a review of properties, history of use and human tolerance, and results of multiple safety studies. *Food Chem. Toxicol.* **40**: 871–898.
27. Seshima, H., Yoshinari, M., Takemoto, S., Hattori, M., Kawada, E., Inoue, T. and Oda, Y. 2006. Control of bisphosphonate release using hydroxyapatite granules. *J. Biomed. Mater. Res. B Appl. Biomater.* **78**: 215–221.
28. Suda, T. 2007. Mechanism of calcification. pp. 145–174. *In*: Bone Biology, 1st ed., Ishiyaku publishers, Tokyo.
29. Sum, A. K., Faller, R. and de Pablo, J. J. 2003. Molecular simulation study of phospholipid bilayers and insights of the interactions with disaccharides. *Biophys. J.* **85**: 2830–2844.
30. Talal, A., Waheed, N., Al-Masri, M., McKay, I. J., Tanner, K. E. and Hughes, F. J. 2009. Absorption and release of protein from hydroxyapatite-polylactic acid (HA-PLA) membranes. *J. Dent.* **37**: 820–826.
31. Tazaki, J., Murata, M., Akazawa, T., Yamamoto, M., Ito, K., Arisue, M., Shibata, T. and Tabata, Y. 2009. BMP-2 release and dose-response studies in hydroxyapatite and beta-tricalcium phosphate. *Biomed. Mater. Eng.* **19**: 141–146.
32. Wassell, D. T., Hall, R. C. and Embery, G. 1995. Adsorption of bovine serum albumin onto hydroxyapatite. *Biomaterials* **16**: 697–702.
33. Willart, J. F., Hedoux, A., Guinet, Y., Danede, F., Paccou, L., Capet, F. and Descamps, M. 2006. Metastability release of the form alpha of trehalose by isothermal solid state vitrification. *J. Phys. Chem. B* **110**: 11040–11043.
34. Wronski, T. J. 2001. Skeletal effects of systemic treatment with basic fibroblast growth factor. *J. Musculoskelet. Neuronal. Interact.* **2**: 9–14.
35. Yamaguchi, A., Komori, T. and Suda, T. 2000. Regulation of osteoblast differentiation mediated by bone morphogenetic proteins, hedgehogs, and Cbfa1. *Endocr. Rev.* **21**: 393–411.
36. Ziegler, J., Mayr-Wohlfart, U., Kessler, S., Breitig, D. and Gunther, K. P. 2002. Adsorption and release properties of growth factors from biodegradable implants. *J. Biomed. Mater. Res.* **59**: 422–428.

Biochemical and Biophysical Research Communications 409 (2011) 260–265

Contents lists available at ScienceDirect

Biochemical and Biophysical Research Communications

journal homepage: www.elsevier.com/locate/ybbrc

Harmine promotes osteoblast differentiation through bone morphogenetic protein signaling

Takayuki Yonezawa [a,b], Ji-Won Lee [b], Ayaka Hibino [c], Midori Asai [c], Hironori Hojo [d], Byung-Yoon Cha [b], Toshiaki Teruya [b,e], Kazuo Nagai [b,c], Ung-Il Chung [d], Kazumi Yagasaki [a,f], Je-Tae Woo [a,b,c,*]

[a] Department of Nutriproteomics, Graduate School of Medicine, The University of Tokyo, 7-3-1 Hongo, Bunkyo-ku, Tokyo 113-0033, Japan
[b] Research Institute for Biological Functions, Chubu University, 1200 Matsumoto, Kasugai, Aichi 487-8501, Japan
[c] Department of Biological Chemistry, College of Bioscience and Biotechnology, Chubu University, 1200 Matsumoto, Kasugai, Aichi 487-8501, Japan
[d] Center for Disease Biology and Integrative Medicine, Faculty of Medicine, The University of Tokyo, 7-3-1 Hongo, Bunkyo-ku, Tokyo 113-0033, Japan
[e] Faculty of Education, University of the Ryukyus, 1 Senbaru, Nishihara, Okinawa 903-0213, Japan
[f] Division of Applied Biological Chemistry, Institute of Agriculture, Tokyo Noko University, 3-5-8 Saiwai, Fuchu, Tokyo 183-8509, Japan

ARTICLE INFO

Article history:
Received 2 May 2011
Available online 6 May 2011

Keywords:
Harmine
Osteoblast
Bone morphogenetic protein
Natural small molecule

ABSTRACT

Bone mass is regulated by osteoblast-mediated bone formation and osteoclast-mediated bone resorption. We previously reported that harmine, a β-carboline alkaloid, inhibits osteoclast differentiation and bone resorption *in vitro* and *in vivo*. In this study, we investigated the effects of harmine on osteoblast proliferation, differentiation and mineralization. Harmine promoted alkaline phosphatase (ALP) activity in MC3T3-E1 cells without affecting their proliferation. Harmine also increased the mRNA expressions of the osteoblast marker genes *ALP* and *Osteocalcin*. Furthermore, the mineralization of MC3T3-E1 cells was enhanced by treatment with harmine. Harmine also induced osteoblast differentiation in primary calvarial osteoblasts and mesenchymal stem cell line C3H10T1/2 cells. Structure–activity relationship studies using harmine-related β-carboline alkaloids revealed that the C3–C4 double bond and 7-hydroxy or 7-methoxy group of harmine were important for its osteogenic activity. The bone morphogenetic protein (BMP) antagonist noggin and its receptor kinase inhibitors dorsomorphin and LDN-193189 attenuated harmine-promoted ALP activity. In addition, harmine increased the mRNA expressions of *Bmp-2*, *Bmp-4*, *Bmp-6*, *Bmp-7* and its target gene *Id1*. Harmine also enhanced the mRNA expressions of *Runx2* and *Osterix*, which are key transcription factors in osteoblast differentiation. Furthermore, BMP-responsive and Runx2-responsive reporters were activated by harmine treatment. Taken together, these results indicate that harmine enhances osteoblast differentiation probably by inducing the expressions of BMPs and activating BMP and Runx2 pathways. Our findings suggest that harmine has bone anabolic effects and may be useful for the treatment of bone-decreasing diseases and bone regeneration as a lead compound.

1. Introduction

Bone mass is controlled by continuous bone remodeling through osteoblastic bone formation and osteoclastic bone resorption. Abnormalities in bone remodeling can produce a variety of bone-decreasing disorders such as osteoporosis, hypercalcemia, rheumatoid arthritis, tumor metastasis into bone, periodontitis and Paget's disease [1]. Although some anti-resorptive drugs including bisphosphonates and selective estrogen receptor modulators are available, anabolic drugs that aggressively promote osteoblastogenesis and bone formation are insufficient for effective treatment of these diseases. In addition, the development of osteogenic agents is desired for bone regeneration therapy.

Osteoblasts are derived from mesenchymal stem cells, which can also differentiate into chondrocytes, adipocytes and myoblasts [2]. Alkaline phosphatase (ALP) and bone matrix proteins such as osteocalcin are produced by osteoblasts, and are related to the induction of osteoblastic mineralization. Bone morphogenetic proteins (BMPs) are the most potent inducer cytokines of osteoblastogenesis [3]. Through binding to type I and type II serine/threonine kinase receptors, BMPs activate the transcription factor Smad, which translocates into the nucleus and modulates the expression of many target genes [4,5]. Runt-related transcription factor 2 (Runx2) and Osterix are known to be essential transcription factors for osteoblast differentiation. Gene knockout mice for Runx2 and

* Corresponding author at: Department of Biological Chemistry, College of Bioscience and Biotechnology, Chubu University, 1200 Matsumoto, Kasugai, Aichi 487-8501, Japan. Fax: +81 568 52 6594.
E-mail address: jwoo@isc.chubu.ac.jp (J.-T. Woo).

0006-291X/$ - see front matter © 2011 Elsevier Inc. All rights reserved.
doi:10.1016/j.bbrc.2011.05.001

Osterix exhibit a complete defect in bone formation [6–9]. BMPs were also reported to activate these transcription factors for osteoblast differentiation [10]. Thus, BMPs have been developed as bone anabolic agents and approved for clinical use [11]. However, these agents have some inadequacies, including limited use for local applications, high costs and difficulty in delivery [12]. Therefore, small molecules that stimulate the production or signaling pathways of BMPs may be useful to resolve these problems.

Harmine is a naturally occurring β-carboline alkaloid compound found in various plants including *Peganum harmala* (Syrian Rue) and *Passiflora incarnata* (Passionflower) [13]. It was reported to have diverse pharmacological actions such as inhibition of monoamine oxidase (MAO), improvement of insulin sensitivity and a vasorelaxant effect [14–16]. Recently, we demonstrated that harmine prevented bone loss *in vitro* and *in vivo* by suppressing osteoclastogenesis [17]. In the present study, we found that harmine promotes osteoblast differentiation and mineralization via BMP signaling pathways accompanied by upregulation of Runx2 and Osterix.

2. Materials and methods

2.1. Reagents

Harmine, harmol, harmane, harmaline, harmalol, recombinant human BMP-2, recombinant human noggin, dorsomorphin, LDN-193189 and Alizarin red S were purchased from Wako Pure Chemical Industries Ltd. (Osaka, Japan). Fast blue BB salt, naphthol AS-MX phosphate, Dulbecco's modified Eagle's medium (DMEM) and fetal bovine serum (FBS) were purchased from Sigma Chemicals Co. (St. Louis, MO). α-MEM was purchased from Invitrogen (Carlsbad, CA). Reporter plasmids encoding 12xGCCG-Luc and 6xOSE2-Luc were generous gifts from Dr. T. Katagiri (Saitama Medical School) and Dr. G. Karsenty (Columbia University), respectively. All other reagents were obtained from Sigma Chemical Co. or Wako Pure Chemical Industries Ltd.

2.2. Animals

Four- to six-week-old ddY mice were purchased from SLC Inc. (Shizuoka, Japan). The experimental procedures and housing conditions for the animals were approved by the Animal Experiment Committee of Chubu University. All animals were cared for and treated humanely in accordance with the Guidelines for Experiments using Animals of Chubu University.

2.3. Cell cultures

MC3T3-E1 cells, an osteoblastic cell line from neonatal mouse calvaria, and C3H10T1/2 cells, mesenchymal stem cell-like fibroblasts, were obtained from the RIKEN Cell Bank (Tsukuba, Japan). MC3T3-E1 and C3H10T1/2 cells were cultured in α-MEM and DMEM supplemented with 10% FBS, respectively. Primary calvarial osteoblasts were obtained from the calvariae of neonatal ddY mice and maintained in α-MEM containing 10% FBS as described previously [18].

2.4. Osteoblast differentiation

The cells were seeded in 96-well plates (5×10^3 cells/well) and cultured for 2 days. After reaching confluency, the cells were further incubated with samples for 7 days. Ascorbic acid (50 μg/ml) and β-glycerophosphate (10 mM) were supplemented in the cultures of C3H10T1/2 cells and primary osteoblasts. Cytotoxicity was determined using a Cell-Counting Kit 8 (Dojindo, Kumamoto, Japan) according to the manufacturer's protocol. For proliferation assays, the cells were seeded in 96-well plates (2×10^3 cells/well) and cultured with compounds for 2 days. The relative cell numbers were determined by the MTT assay.

2.5. ALP activity assay and staining

After culture, the cells were fixed with ice-cold 100% methanol. For measurement of the ALP activity, the fixed cells were incubated in ALP substrate buffer (100 mM Tris–HCl pH 8.5, 2 mM $MgCl_2$, 6.6 mM 4-nitrophenyl phosphate) for 30–120 min. The absorbance at 410 nm was measured as the ALP activity using a microplate reader. For ALP staining, the fixed cells were incubated in ALP staining buffer (100 mM Tris–HCl pH 8.5, 2 mM MgCl2, 1% *N,N*-dimethylformamide, 0.01% naphthol AS-MX phosphate and 0.06% fast blue BB salt.

2.6. Real-time reverse transcription-polymerase chain reaction (RT-PCR) analysis

MC3T3-E1 cells were cultured with or without harmine for 4 and 7 days. Total RNA was isolated using ISOGEN (Nippon Gene, Toyama, Japan) and cDNA was synthesized using a ReverTra Ace qPCR RT kit (Toyobo, Osaka, Japan), according to the manufacturer's instructions. Real-time PCR was performed with FastStart SYBR Green Master (Roche Diagnostics, Mannheim, Germany) in an ABI Prism 7500 Sequence Detection System (Applied Biosystems, Foster City, CA) in triplicate. The primer sequences are available upon request. The relative expression levels of target genes against the endogenous reference glyceraldehyde 3-phosphate dehydrogenase (GAPDH) were calculated using the delta cycle threshold (Ct) method.

2.7. Osteocalcin enzyme immunoassay (EIA)

MC3T3-E1 cells were cultured with ascorbic acid (50 μg/ml) and β-glycerophosphate (10 mM) for 14 days. The Osteocalcin concentrations in the culture media were measured using an osteocalcin EIA kit (Biomedical Technologies Inc., Stoughton, MA).

2.8. Mineralization assay

MC3T3-E1 cells were cultured under the same conditions used for the osteocalcin EIA assay. Mineralization of the extracellular matrix was determined by Alizarin red S staining and von Kossa staining, which detect calcium. After cell fixation, 1% Alizarin red S solution was added and incubated for 30–60 min at room temperature. In other wells, the cultured cells were incubated with 5% silver nitrate under UV light for 1 h, followed by 5% sodium thiosulfate for 5 min.

2.9. Reporter gene assays

MC3T3-E1 cells were seeded onto 48-well plates and allowed to reach approximately 80% confluency. The cells were then transfected with 0.1 μg of reporter plasmids containing BMP-responsive elements (12xGCCG-Luc) [19] or Runx2-responsive elements (6xOSE2-Luc) [20] and 0.01 μg of control reporter plasmids encoding TK-Renilla luciferase (Promega, Madison, WI) using Lipofectamine LTX (Invitrogen) according to the manufacturer's instructions. After 8 h, the cells were cultured with or without harmine for 60 h. After the culture, the cells were lysed in Passive Lysis Buffer (Promega). Dual luciferase assays were performed using a Dual Luciferase Reporter Assay System (Promega) and a Glomax 96 Microplate Luminometer (Promega). All measurements were carried out on triplicate samples.

2.10. Statistical analysis

All data are expressed as the mean ± SD. Statistical analyses of the significance of differences among values were carried out by one-way ANOVA with a post hoc Dunnett's test or Student's *t*-test. Values of $P < 0.05$ were considered to indicate statistical significance.

3. Results and discussion

3.1. Effects of harmine on osteoblast differentiation in MC3T3-E1 cells

To evaluate the effects of harmine on osteoblast differentiation, staining for ALP was performed as an early-differentiation marker of osteoblasts using MC3T3-E1 cells, a preosteoblastic cell line derived from newborn mouse calvaria. The results showed that harmine dose-dependently enhanced the intensity of ALP staining (Fig. 1A). Harmine also increased the mRNA expression of *Alp* (Fig. 1B). Next, the mRNA expression of *Osteocalcin* was measured as a late-stage marker of osteoblast differentiation. Treatment with harmine significantly increased the expression of *Osteocalcin* compared with control cells (Fig. 1B). The effects of harmine on osteocalcin protein production were determined by an EIA. Osteocalcin in the culture media was elevated after treatment with harmine (Fig. 1C), indicating that harmine enhanced osteocalcin protein production. To determine osteoblastic mineralization, MC3T3-E1 cells were cultured with harmine in the presence of ascorbic acid and β-glycerophosphate for 14 days. Harmine dramatically increased the mineralized area visualized by Alizarin red S staining for calcium (Fig. 1D). Similar results were obtained after von Kossa staining (Fig. 1E). In addition, a proliferation assay was performed to clarify whether the osteogenic effects of harmine were dependent on cell proliferation. However, harmine did not affect the total cell number (data not shown). These findings indicate that harmine promotes the early and late stages of osteoblast differentiation.

3.2. Effects of harmine on osteoblast differentiation in primary calvarial osteoblasts and mesenchymal stem cell line C3H10T1/2 cells

We confirmed the effects of harmine on osteoblast differentiation using primary calvarial osteoblasts. Harmine significantly enhanced the ALP activity (Fig. 2A) and promoted the mineralization (Fig. 2B) in primary calvarial osteoblasts. To determine whether harmine acts on more primitive cells, we investigated its effects on the ALP activity in mouse mesenchymal stem cell line C3H10T1/2 cells. As shown in Fig. 2C, harmine also significantly enhanced the ALP activity in C3H10T1/2 cells. These findings suggest that harmine stimulates the differentiation of both osteoblast-committed cell and mesenchymal stem cells into osteoblasts.

3.3. Structure–activity relationships of β-carboline alkaloids with the ALP activity

Harmine is a member of the β-carboline alkaloids possessing a common tricyclic pyrido[3,4-b] indole structure. To assess the correlation between the chemical structure and the activity of harmine, the effects of its derivatives (Fig. 3A) on ALP activity were compared with the effects of harmine. Harmine dose-dependently

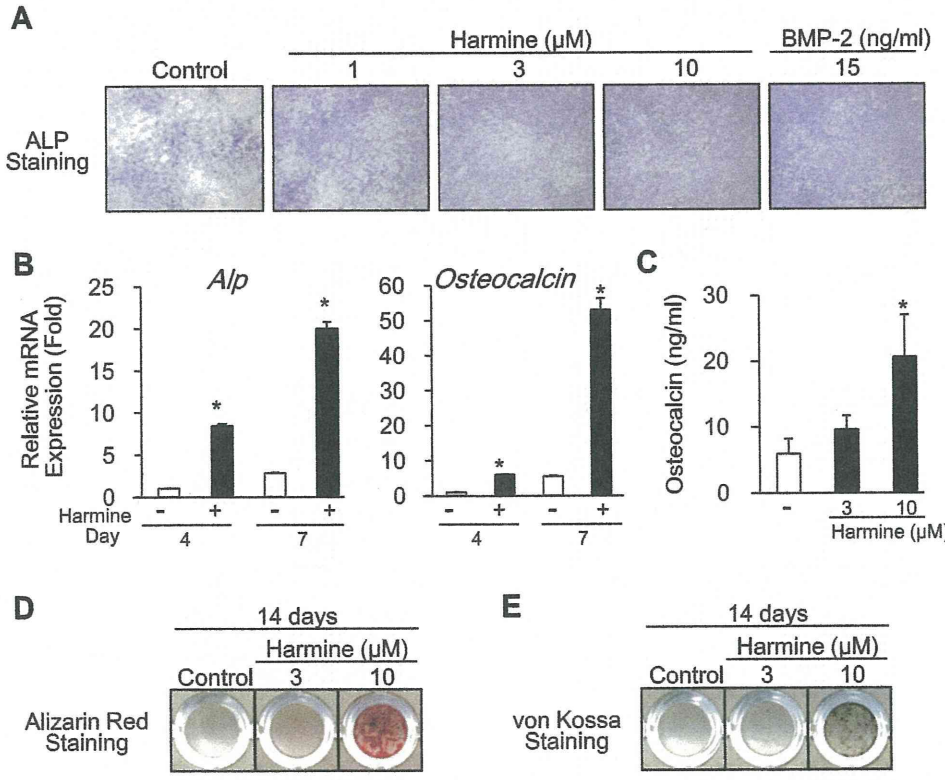

Fig. 1. Effects of harmine on osteoblast differentiation in MC3T3-E1 cells. (A and B) MC3T3-E1 cells were cultured with or without harmine for 7 days (A) or the indicated numbers of days (B) after the cells reached confluency. After the culture, the cells were stained for ALP (A) and the relative expressions of *Alp* and *Osteocalcin* mRNAs were determined by real-time RT-PCR (B). (C–E) MC3T3-E1 cells were cultured with or without harmine in the presence of 50 μg/ml ascorbic acid and 10 mM β-glycerophosphate for 14 days after the cells reached confluency. The concentrations of osteocalcin in the culture media were measured using an osteocalcin EIA kit (C). Osteoblastic mineralization was determined by Alizarin red S staining (D) and von Kossa staining (E). The photographs are representative of more than three independent experiments. The data represent the means ± SD of more than three cultures. *$P < 0.05$ vs. the control cells.

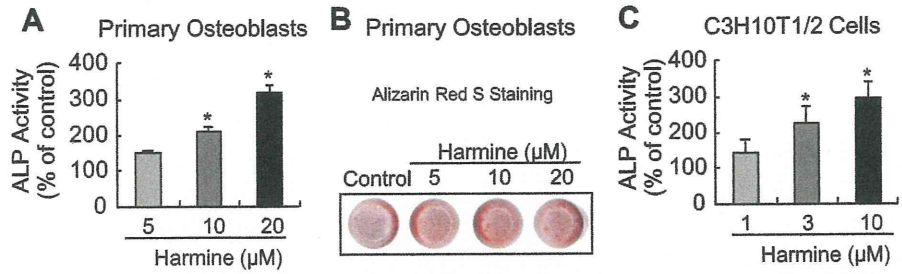

Fig. 2. Effects of harmine on osteoblast differentiation in primary calvarial osteoblasts and C3H10T1/2 cells. (A–C) Primary calvarial osteoblasts (A and B) and C3H10T1/2 cells (C) were cultured with or without harmine in the presence of 50 μg/ml ascorbic acid and 10 mM β-glycerophosphate for 14 or 7 days, respectively. After the culture, the cells were fixed and the ALP activity was measured (A and C). Osteoblastic mineralization was determined by Alizarin red S staining (B). The photographs are representative of more than three independent experiments. The data represent the means ± SD of more than three cultures. *$P < 0.05$ vs. the control cells.

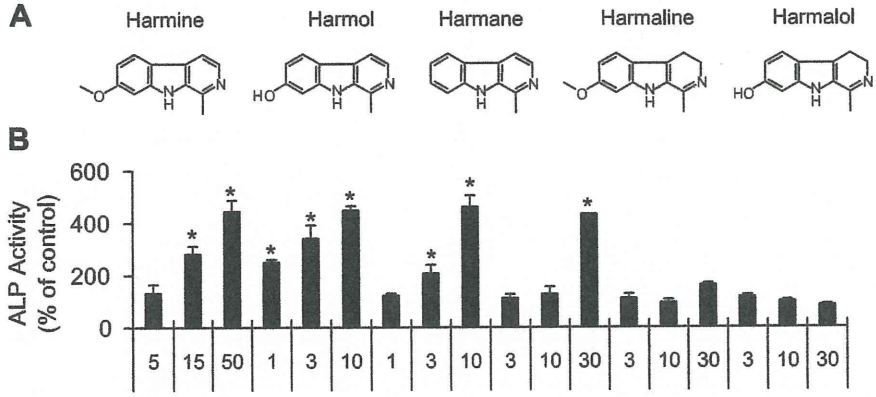

Fig. 3. Effects of β-carboline alkaloids on the ALP activity in MC3T3-E1 cells. (A) Chemical structures of the β-carboline alkaloids. (B) MC3T3-E1 cells were cultured with or without BMP-2 (5–50 ng/ml) or β-carboline alkaloids (1–30 μM) for 7 days. After the culture, the cells were fixed and the ALP activity was measured. The data represent the means ± SD of more than three cultures. *$P < 0.05$ vs. the control cells.

promoted the ALP activity in MC3T3-E1 cells in a similar manner to BMP-2, as a positive control. Harmol, with a methoxy group substituted into the hydroxyl group at position 7, also enhanced the ALP activity at an approximately equal concentration to harmine (Fig. 3B). Weaker promotion of the ALP activity compared with harmine was observed after treatment with harmane, which does not have a substituted group at position 7 (Fig. 3B). Harmaline and harmalol, which have a single bond between C3 and C4, had no effects on the ALP activity at concentrations of up to 30 μM (Fig. 3B). These results for the structure–activity relationships of harmine derivatives on osteoblast differentiation revealed that a double bond between C3 and C4 in the β-carboline structure may be essential for its osteogenic activity. The importance of a methoxy or hydroxy group at position 7 is also suggested by a comparison of the effective concentrations for the ALP activity.

3.4. Involvement of BMP signaling pathways in the effects of harmine on osteoblast differentiation

To clarify the possible participation of BMP signaling pathways in the effects of harmine on osteoblast differentiation, MC3T3-E1 cells were cultured with harmine in the presence of BMP inhibitors, and the ALP activity was measured. The BMP antagonist noggin and type I BMP receptor kinase inhibitors dorsomorphin and LDN-193289 almost completely abolished the harmine-promoted ALP activity (Fig. 4A). These findings indicate that the osteogenic actions of harmine are mediated by BMP signaling pathways. Some osteogenic agents including statins and flavonoids were reported to promote osteoblast differentiation via the induction of BMP expression [12]. Therefore, the mRNA expressions of *Bmp-2*, *Bmp-4*, *Bmp-6* and *Bmp-7* were evaluated. The results revealed that harmine increased the expressions of *Bmp-2*, *Bmp-4*, *Bmp-6* and *Bmp-7* mRNAs at day 7. The *Bmp-7* mRNA expression was elevated as early as at day 4 in response to harmine (Fig. 4B). Next, to elucidate the effects of harmine on BMP signaling, we measured the mRNA expression of inhibitor of DNA-binding 1 (*Id1*), which is known to be a target gene of BMPs [4]. The mRNA expression of *Id1* was higher in harmine-treated cells than in control cells (Fig. 4B). These findings indicate that harmine promotes the expressions of BMPs and activates downstream signaling pathways of BMPs. Runx2 and Osterix are crucial transcription factors for osteoblast differentiation and were reported to be induced by BMPs [10]. Treatment with harmine also promoted the expressions of *Runx2* and *Osterix* mRNAs (Fig. 4B). To confirm the possible involvement of BMP- and Runx2-dependent signaling in the effects of harmine, luciferase assays were performed using a BMP-responsive reporter (12xGCCG-Luc), which has Smad-binding motifs, and a Runx2-responsive reporter (6xOSE2-Luc), which has Runx2-binding motifs. Both reporters were significantly activated in response to harmine (Fig. 4C). Thus, harmine may promote osteoblast differentiation through the induction of BMPs, and subsequent activation of BMP-Smad and Runx2 signaling pathways.

β-Carboline alkaloids were reported to have many pharmacological actions, including inhibition of MAO-A, inhibition of cyclin-dependent kinases (CDKs), binding to serotonin receptor 2A (5-HT2A), binding to the imidazoline I_2 receptor and binding to the benzodiazepine-binding site on the $GABA_A$ receptor [14]. However, authentic MAO inhibitors (tranylcypromine, clorgyline and pargyline) and a CDK inhibitor (roscovitine) did not enhance

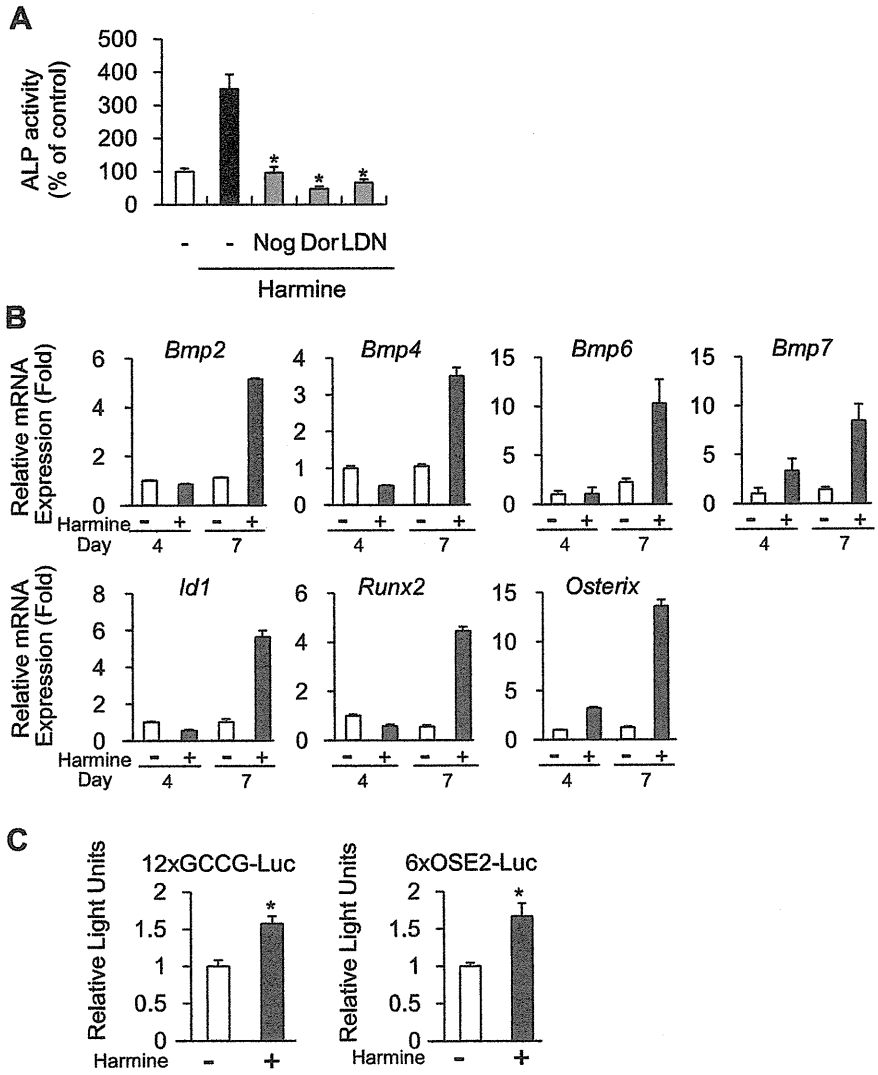

Fig. 4. Effects of harmine on BMP-related signaling pathways. (A) MC3T3-E1 cells were cultured with the BMP inhibitors noggin (Nog; 100 ng/ml), dorsomorphin (Dor; 0.5 μM) or LDN-193189 (LDN; 0.2 μM) in the presence of harmine (10 μM) for 7 days. After the culture, the cells were fixed and the ALP activity was measured. The data represent the means ± SD of three or more determinations. *$P < 0.05$ vs. the harmine-treated cells without an inhibitor. (B) MC3T3-E1 cells were cultured with or without harmine (10 μM) for the indicated numbers of days after the cells reached confluency. The relative mRNA expressions of *Bmp-2*, *Bmp-4*, *Bmp-6*, *Bmp-7*, *Id1*, *Runx2* and *Osterix* were determined by real-time RT-PCR. (C) MC3T3-E1 cells were transiently transfected with a BMP-responsive reporter (12xGCCG-Luc) or a Runx2-responsive reporter (6xOSE2-Luc) and treated with harmine (10 μM) for 60 h. After the culture, the cells were lysed and the luciferase activities were measured. The data represent the means ± SD of triplicate determinations. *$P < 0.05$ vs. the control cells.

the ALP activity in MC3T3-E1 cells in the present study (data not shown). In addition, none of the agonists or antagonists against 5-HT2A (TCB2 and ketanserin), I_2 receptor (clonidine, 2-BFI and BU 224) or $GABA_A$ receptor (THIP and bicuculline) had any effects on osteoblast differentiation (data not shown). These findings indicate that the osteogenic effects of harmine may not be related to these target molecules.

In summary, we have found novel osteogenic actions of harmine in addition to the suppression of osteoclastogenesis described in our recent report [17]. Harmine promotes osteoblast differentiation and mineralization accompanied by increases in ALP and osteocalcin expression via the induction of BMPs and Runx2. We previously showed that harmine suppressed ovariectomy-induced bone loss in mice; however, the osteogenic potency of harmine might have contributed to the suppression of bone loss. Although further studies are required to clarify the *in vivo* actions and mechanisms, harmine may become a superior drug candidate for the treatment of bone-decreasing diseases, since it is expected to not only enhance bone formation but also suppress bone resorption.

Acknowledgments

We thank Drs. T. Katagiri and G. Karsenty for their kind provision of experimental materials. This work was partly supported by a Grant-in-Aid for Scientific Research from the Ministry of Education, Culture, Sports, Science and Technology (No. 19380077). This study was performed at a laboratory that is supported by an endowment from Erina Co. Inc. (Tokyo, Japan).

References

[1] G.A. Rodan, T.J. Martin, Therapeutic approaches to bone diseases, Science 289 (2000) 1508–1514.

[2] S. Harada, G.A. Rodan, Control of osteoblast function and regulation of bone mass, Nature 423 (2003) 349–355.
[3] A. Yamaguchi, T. Komori, T. Suda, Regulation of osteoblast differentiation mediated by bone morphogenetic proteins, hedgehogs, and Cbfa1, Endocr. Rev. 21 (2000) 393–411.
[4] K. Miyazono, S. Maeda, T. Imamura, BMP receptor signaling: transcriptional targets, regulation of signals, and signaling cross-talk, Cytokine Growth Factor Rev. 16 (2005) 251–263.
[5] E. Canalis, A.N. Economides, E. Gazzerro, Bone morphogenetic proteins, their antagonists, and the skeleton, Endocr. Rev. 24 (2003) 218–235.
[6] P. Ducy, R. Zhang, V. Geoffroy, A.L. Ridall, G. Karsenty, Osf2/Cbfa1: a transcriptional activator of osteoblast differentiation, Cell 89 (1997) 747–754.
[7] T. Komori, H. Yagi, S. Nomura, A. Yamaguchi, K. Sasaki, K. Deguchi, Y. Shimizu, R.T. Bronson, Y.H. Gao, M. Inada, M. Sato, R. Okamoto, Y. Kitamura, S. Yoshiki, T. Kishimoto, Targeted disruption of Cbfa1 results in a complete lack of bone formation owing to maturational arrest of osteoblasts, Cell 89 (1997) 755–764.
[8] F. Otto, A.P. Thornell, T. Crompton, A. Denzel, K.C. Gilmour, I.R. Rosewell, G.W. Stamp, R.S. Beddington, S. Mundlos, B.R. Olsen, P.B. Selby, M.J. Owen, Cbfa1, a candidate gene for cleidocranial dysplasia syndrome, is essential for osteoblast differentiation and bone development, Cell 89 (1997) 765–771.
[9] K. Nakashima, X. Zhou, G. Kunkel, Z. Zhang, J.M. Deng, R.R. Behringer, B. de Crombrugghe, The novel zinc finger-containing transcription factor osterix is required for osteoblast differentiation and bone formation, Cell 108 (2002) 17–29.
[10] P.J. Marie, Transcription factors controlling osteoblastogenesis, Arch. Biochem. Biophys. 473 (2008) 98–105.
[11] T.W. Axelrad, T.A. Einhorn, Bone morphogenetic proteins in orthopaedic surgery, Cytokine Growth Factor Rev. 20 (2009) 481–488.
[12] I.R. Garrett, Anabolic agents and the bone morphogenetic protein pathway, Curr. Top. Dev. Biol. 78 (2007) 127–171.
[13] J.R.F. Allen, B.R. Holmstedt, The simple β-carboline alkaloids, Phytochemistry 19 (1980) 1573–1582.
[14] R. Cao, W. Peng, Z. Wang, A. Xu, β-Carboline alkaloids: biochemical and pharmacological functions, Curr. Med. Chem. 14 (2007) 479–500.
[15] H. Waki, K.W. Park, N. Mitro, L. Pei, R. Damoiseaux, D.C. Wilpitz, K. Reue, E. Saez, P. Tontonoz, The small molecule harmine is an antidiabetic cell-type-specific regulator of PPARγ expression, Cell Metab. 5 (2007) 357–370.
[16] H. Berrougui, C. Martin-Cordero, A. Khalil, M. Hmamouchi, A. Ettaib, E. Marhuenda, M.D. Herrera, Vasorelaxant effects of harmine and harmaline extracted from *Peganum harmala* L. seeds in isolated rat aorta, Pharmacol. Res. 54 (2006) 150–157.
[17] T. Yonezawa, S. Hasegawa, M. Asai, T. Ninomiya, T. Sasaki, B.Y. Cha, T. Teruya, H. Ozawa, K. Yagasaki, K. Nagai, J.T. Woo, Harmine, a β-carboline alkaloid, inhibits osteoclast differentiation and bone resorption in vitro and in vivo, Eur. J. Pharmacol. 650 (2011) 511–518.
[18] N. Takahashi, N. Udagawa, Y. Kobayashi, T. Suda, Generation of osteoclasts in vitro, and assay of osteoclast activity, Methods Mol. Med. 135 (2007) 285–301.
[19] K. Kusanagi, H. Inoue, Y. Ishidou, H.K. Mishima, M. Kawabata, K. Miyazono, Characterization of a bone morphogenetic protein-responsive Smad-binding element, Mol. Biol. Cell 11 (2000) 555–565.
[20] P. Ducy, G. Karsenty, Two distinct osteoblast-specific cis-acting elements control expression of a mouse osteocalcin gene, Mol. Cell. Biol. 15 (1995) 1858–1869.

Journal of Bioscience and Bioengineering
VOL. 113 No. 2, 252–257, 2012

ELSEVIER

www.elsevier.com/locate/jbiosc

Evaluation of the implant type tissue-engineered cartilage by scanning acoustic microscopy

Yoko Tanaka,[1] Yoshifumi Saijo,[2] Yuko Fujihara,[1] Hisayo Yamaoka,[1] Satoru Nishizawa,[1] Satoru Nagata,[3] Toru Ogasawara,[4] Yukiyo Asawa,[1] Tsuyoshi Takato,[4] and Kazuto Hoshi[1,*]

Department of Cartilage & Bone Regeneration (Fujisoft), Graduate School of Medicine, The University of Tokyo, Hongo 7-3-1, Bunkyo-ku, Tokyo 113-8655, Japan,[1] Department of Biomedical Measurements, Smart Aging International Research Center, Tohoku University, Seiryo-machi 4–1, Aoba-ku Sendai, Miyagi, 980–8575, Japan,[2] Nagata Microtia and Reconstructive Plastic Surgery Clinic, Sasameminami-cho 22–1, Toda-shi, Saitama 335–0035, Japan,[3] and Departments of Sensory & Motor System Medicine, Graduate School of Medicine, The University of Japan, Hongo 7-3-1, Bunkyo-ku, Tokyo 113–8655, Japan[4]

Received 19 May 2011; accepted 11 October 2011
Available online 3 December 2011

The tissue-engineered cartilages after implantation were nonuniform tissues which were mingling with biodegradable polymers, regeneration cartilage and others. It is a hard task to evaluate the biodegradation of polymers or the maturation of regenerated tissues in the transplants by the conventional examination. Otherwise, scanning acoustic microscopy (SAM) system specially developed to measure the tissue acoustic properties at a microscopic level. In this study, we examined acoustic properties of the tissue-engineered cartilage using SAM, and discuss the usefulness of this devise in the field of tissue engineering. We administered chondrocytes/atelocollagen mixture into the scaffolds of various polymers, and transplanted the constructs in the subcutaneous areas of nude mice for 2 months. We harvested them and examined the sound speed and the attenuation in the section of each construct by the SAM. As the results, images mapping the sound speed exhibited homogenous patterns mainly colored in blue, in all the tissue-engineered cartilage constructs. Contrarily, the images of the attenuation by SAM showed the variation of color ranged between blue and red. The low attenuation area colored in red, which meant hard materials, were corresponding to the polymer remnant in the toluidine blue images. The localizations of blue were almost similar with the metachromatic areas in the histology. In conclusion, the SAM is regarded as a useful tool to provide the information on acoustic properties and their localizations in the transplants that consist of heterogeneous tissues with various components.

[**Key words:** Tissue-engineering; Cartilage; Acoustic microscopy; Biodegradable polymer; Scaffold]

The autologous chondrocyte transplantation (ACT) has already been available for clinical use. However, the present applications are confined to the treatment for focal cartilage defects (1–4). To broaden the clinical application of the cartilage regenerative medicine, many researchers have made efforts to develop an implant-type tissue-engineered cartilage with firmness and 3-D structure (5–10), and attempted to apply the porous biodegradable polymer scaffolds (11–22). The materials of the biodegradable polymers included PLLA (22–25) and others, each of which showed different biocompatibility and biodegradability. In the experiments of previous studies, although some of the tissue-engineered cartilage constructs using the porous biodegradable polymer scaffolds had been originally block-shaped, they became edging off and shrunk during the in vivo transplantation. This kind of deformity may be caused by the imbalance between degradation of the porous scaffolds and tissue maturation of the tissue-engineered cartilage. The deformity of the transplants directly affects clinical outcome or patient satisfaction in the clinical situation. Therefore, the biodegradation of polymer scaffolds should be synchronized with the cartilage regeneration in the implant-type tissue-engineered cartilage (26).

To establish such ideal biodegradable scaffold, we need to evaluate the biodegradation of scaffolds in the body, and should know the alteration of the mechanical properties of polymers. However, we principally conducted histological or biochemical examinations to detect the remaining of polymers in the body, and the information on mechanical properties could not be taken from these methods. The detailed analyses on the mechanical properties of the polymer scaffolds in the tissue-engineered constructs transplanted in the body are hard tasks by conventional measurement, such as an indentation device. In the case of the tissue-engineered cartilage using the biodegradable scaffold, the constructs were the hybrid of artificial polymers and regenerative tissues, and were heterogeneous in contents. Although we had usually measured the mechanical properties of tissue-engineered cartilage by the indentation device, only those of the whole constructs, but not of the polymer scaffolds, could be obtained.

* Correspondence author. Tel.: +81 3 3815 5411x37386; fax: +81 3 5800 9891.
E-mail address: pochi-tky@umin.net (K. Hoshi).

1389-1723/$ - see front matter © 2011, The Society for Biotechnology, Japan. All rights reserved.
doi:10.1016/j.jbiosc.2011.10.011